Appendix P: Compilation of Surface Creep on California Faults and Comparison of WGCEP 2007 Deformation Model to Pacific-North American Plate Motion

By Beth A. Wisely[1], David A. Schmidt[1], and Ray J. Weldon II[1]

USGS Open File Report 2007-1437P
CGS Special Report 203P
SCEC Contribution #1138P
Version 1.0

2008

U.S. Department of the Interior
U.S. Geological Survey

California Department of Conservation
California Geological Survey

[1]**University of Oregon, Eugene**

U.S. Department of the Interior
DIRK KEMPTHORNE, Secretary

U.S. Geological Survey
Mark D. Myers, Director

State of California
ARNOLD SCHWARZENEGGER, Governor

The Resources Agency
MIKE CHRISMAN, Secretary for Resources

Department of Conservation
Bridgett Luther, Director

California Geological Survey
John G. Parrish, Ph.D., State Geologist

U.S. Geological Survey, Reston, Virginia 2008

For product and ordering information:
World Wide Web: http://www.usgs.gov/pubprod
Telephone: 1-888-ASK-USGS

For more information on the USGS—the Federal source for science about the Earth,
its natural and living resources, natural hazards, and the environment:
World Wide Web: http://www.usgs.gov
Telephone: 1-888-ASK-USGS

Suggested citation:
Wisely, B.A., Schmidt, D.A., and Weldon, R.J, II,. 2008, Compilation of surface creep on California faults and comparison of WGCEP 2007 deformation model to Pacific-North American Plate motion, *Appendix P in* The Uniform California Earthquake Rupture Forecast, version 2 (UCERF 2): U.S. Geological Survey Open-File Report 2007-1437P and California Geological Survey Special Report 203P, 43 p. [http://pubs.usgs.gov/of/2007/1437/p/].

Contents

Introduction:

This Appendix contains 3 sections that 1) documents published observations of surface creep on California faults, 2) constructs line integrals across the WG-07 deformation model to compare to the Pacific – North America plate motion, and 3) constructs strain tensors of volumes across the WG-07 deformation model to compare to the Pacific – North America plate motion.

Observation of creep on faults is a critical part of our earthquake rupture model because if a fault is observed to creep the moment released as earthquakes is reduced from what would be inferred directly from the fault's slip rate. There is considerable debate about how representative creep measured at the surface during a short time period is of the whole fault surface through the entire seismic cycle (e.g. *Hudnut and Clark,* 1989). Observationally, it is clear that the amount of creep varies spatially and temporally on a fault. However, from a practical point of view a single creep rate is associated with a fault section and the reduction in seismic moment generated by the fault is accommodated in seismic hazard models by reducing the surface area that generates earthquakes or by reducing the slip rate that is converted into seismic energy. WG-07 decided to follow the practice of past Working Groups and the National Seismic Hazard Map and used creep rate (where it was judged to be interseismic, see Table P1) to reduce the area of the fault surface that generates seismic events. In addition to following past practice, this decision allowed the Working Group to use a reduction of slip rate as a separate factor to accommodate aftershocks, post seismic slip, possible aseismic permanent deformation along fault zones and other processes that are inferred to affect the entire surface area of a fault, and thus are better modeled as a reduction in slip rate. C-zones are also handled by a reduction in slip rate, because they are inferred to include regions of widely distributed shear that is not completely expressed as earthquakes large enough to model.

Because the ratio of the rate of creep relative to the total slip rate is often used to infer the average depth of creep, the "depth" of creep can be calculated and used to reduce the surface area of a fault that generates earthquakes in our model. This reduction of surface area of rupture is described by an "aseismicity factor," assigned to each creeping fault in Appendix A. An aseismicity factor of less than 1 is only assigned to faults that are inferred to creep during the entire interseismic period. A single aseismicity factor was chosen for each section of the fault that creeps by expert opinion from the observations documented here. Uncertainties were not determined for the aseismicity factor, and thus it represents an unmodeled (and difficult to model) source of error. This Appendix simply provides the documentation of known creep, the type and precision of its measurement, and attempts to characterize the creep as interseismic, afterslip, transient or triggered.

Parts 2 and 3 of this Appendix compare the WG-07 deformation model and the seismic source model it generates to the strain generated by the Pacific - North American plate motion. The concept is that plate motion generates essentially all of the elastic strain in the vicinity of the plate boundary that can be released as earthquakes. Adding up the slip rates on faults and all others sources of deformation (such as C-zones and distributed "background" seismicity) should approximately yield the plate motion. This addition is usually accomplished by one of four approaches: 1) line integrals that sum deformation along discrete paths through the deforming zone between the two plates, 2) seismic moment tensors that add up seismic moment of a representative set of earthquakes generated by a crustal volume spanning the plate boundary, 3) strain tensors generated by adding up the strain associated with all of the faults in a crustal volume spanning the plate boundary, and 4) strain measured across the plate boundary by geodesy. In this Appendix we apply approaches 1 and 3. We cannot apply the moment tensor approach because most of the seismic moment released in the historical period in California predates the instrumental period, so we don't know the source parameters needed to determine a seismic moment tensor. The scalar moment of the historical period has been compared to that produced by the source model in the Main Report, and they match to within uncertainties. A geodetically driven deformation model was discussed by the Working Group and several groups were tasked to generate such a model, but no model was completed in time to be included in WG-07. As discussed in detail in Parts 2 and 3 of this Appendix, the strain inferred from the WG-07 model, determined by methods 1 and 3 above, matches the plate motion in both rate and style to 5-10%, well within the uncertainties.

Part One: Surface Creep Observations

Surface creep commonly refers to aseismic fault slip occurring at or near the surface with slip rates on the order of cm/yr or less (*Wesson*, 1988). Fault creep can be continuous in time or consist of a series of steps (creep events). Steady creep that persists for several decades is often referred to as interseismic creep. Accelerated surface slip can also be observed following a major earthquake in which case it is referred to as afterslip. Short-term fluctuations in creep rate that deviate from long-term rates for weeks or months can be referred to as transient creep or triggered creep in the case where a localized stress perturbation is imposed (*Burford*, 1988).

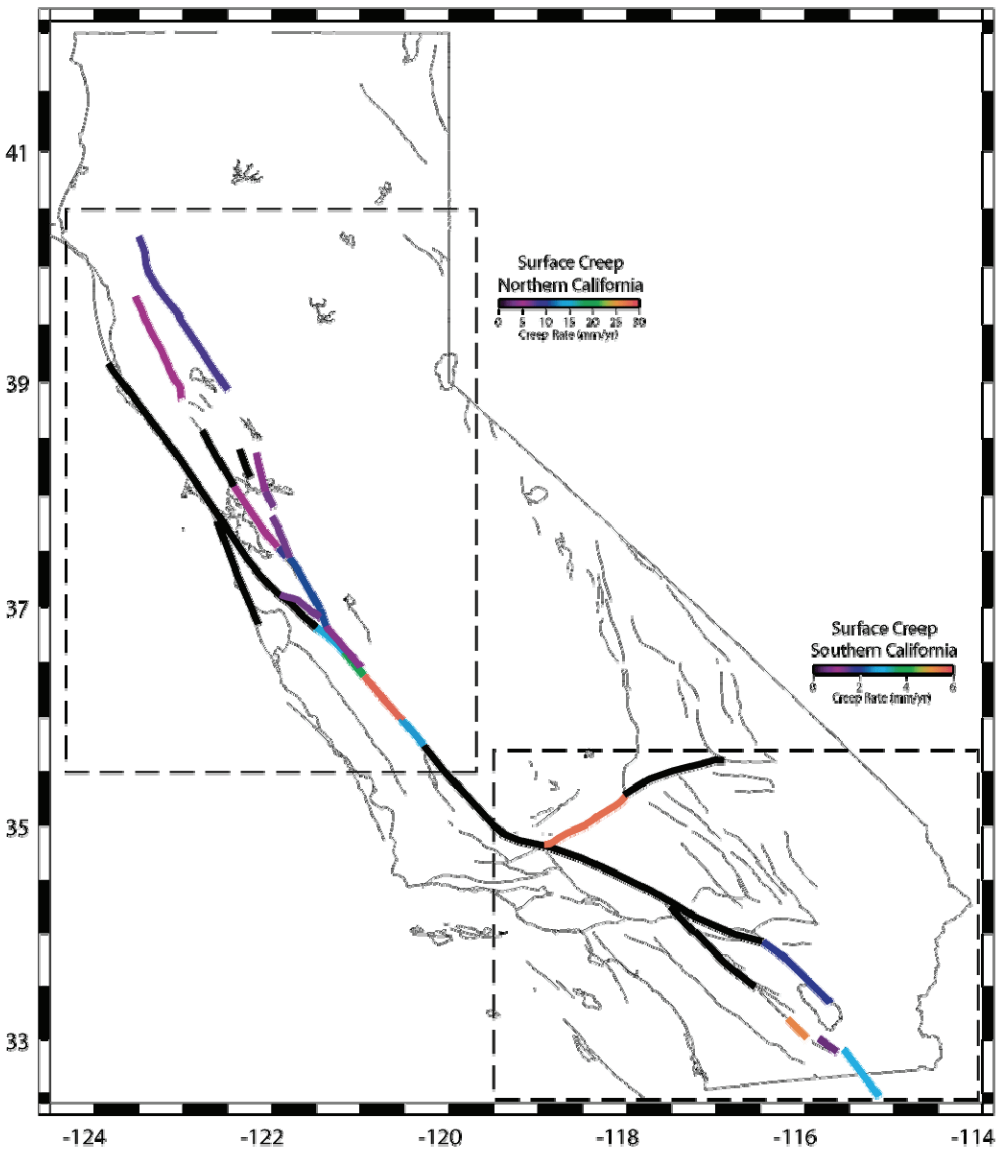

Figure P1 – Map of creep rates of California faults. Note that the color bars representing the range of creep rates are different in northern and southern California. Heavy black lines indicate documented absence of creep. Locations of all known sites with published creep rate observations are shown in more detailed maps of northern and southern California (Figures P2 and P3) and numbers are summarized in Table P1.

Evidence for surface creep is well documented along the San Andreas fault system. Most observations were collected using alignment arrays (*Burford and Harsh*, 1980), creepmeters (*King et al*., 1977), and geodolite networks. Offset cultural features, such as curbs and buildings, provide an additional record of faulting. Occasionally, surface creep is inferred from GPS- or InSAR-derived models of the regional deformation.

In this part of the appendix we summarize the observational data on surface creep along the San Andreas fault system. The two primary sources for this data set include *Louie et al.* (1985) and *Galehouse and Lienkaemper* (2003) for southern and northern California, respectively. These summaries are supplemented with additional sources. We have focused on interseismic observations and have purposefully avoided results that are dominated by transient behavior or otherwise influenced by nearby seismic events. Where multiple observations are available at a particular location, the most consistent observation is used based on the information provided in each source. We have also included data on faults where no surface creep is found despite repeated surveys. Uncertainties are routinely not reported, especially in early work. Occasionally we have inferred an uncertainty from ancillary information in each source or left the uncertainty undefined. A creep rate of zero is recorded in cases where no creep is observed within instrument error.

It is not known if creep is limited to the major branches San Andreas system (with the possible exception of the western Garlock) or simply if these faults slip more rapidly so that creep is evident. Additionally, the San Andreas fault zone has been more intensively surveyed compared to other faults such as those in the Eastern California Shear Zone. Because creep is usually only a fraction of a fault's slip rate it would be very difficult to recognize creep on most Californian faults that have slip rates on the order of mm/yr. Improved instrumentation and newer techniques (e.g. InSAR) will help to better resolve this issue in the future.

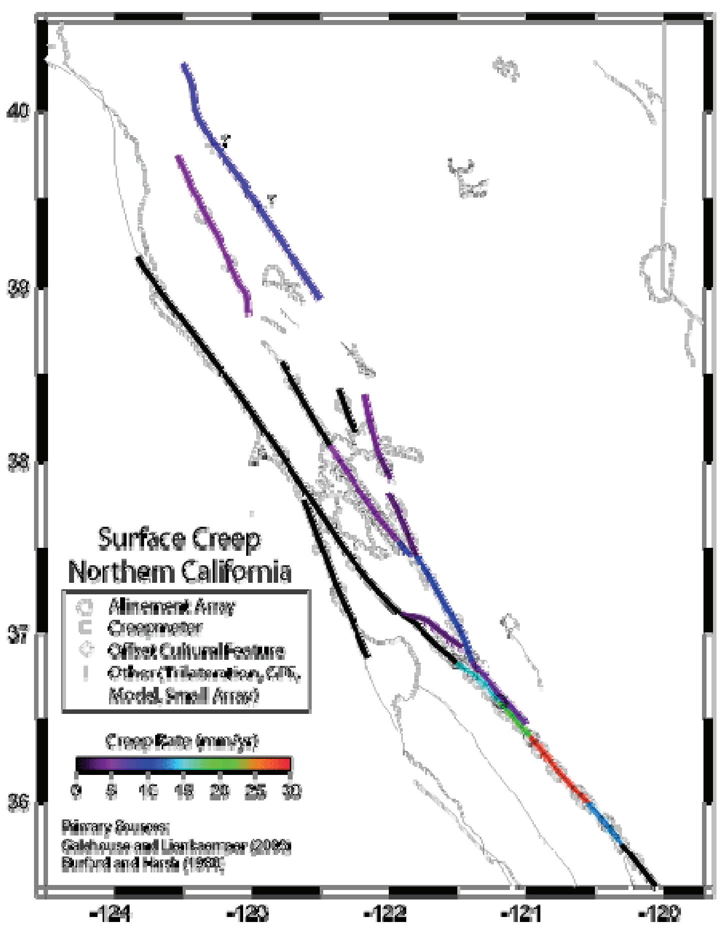

Figure P2 – Detail of creep observations in Northern California. Colors indicate creep rate and bold black lines indicate a documented absence of creep. Small (faint) symbols indicate the locations of creep observations that are summarized in Table P1.

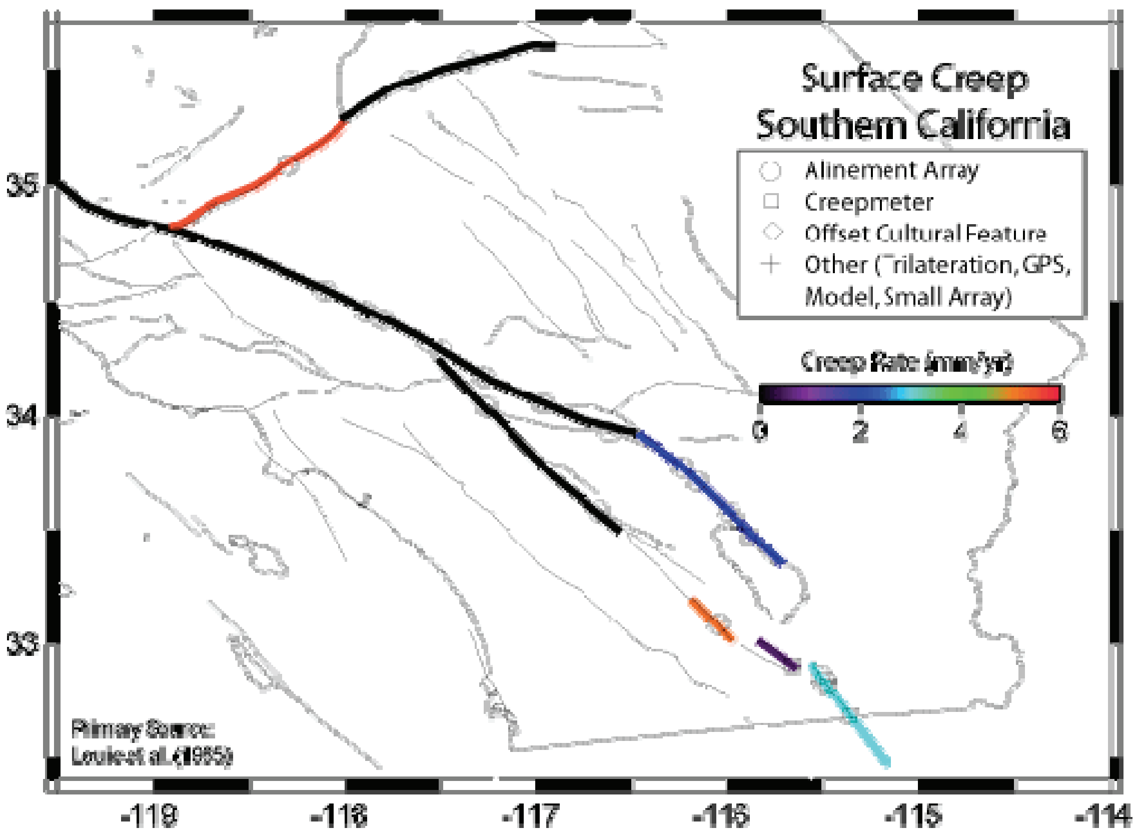

Figure P3 – Detail of creep observations in Southern California. Colors indicate creep rate and bold black lines indicate a documented absence of creep. Small symbols indicate the location of creep observations that are summarized in Table P1.

Table P1: List of surface creep observations in California. Entries are sorted alphabetically by fault name, and then by latitude. Measurement error (sigma) is denoted as 'Und' for undefined when a value is not given by the source. Instrument types are listed as follows: AA=alinement array, CM=creepmeter, Cult=cultural offset features, Geod=small geodetic array, Mod=inferred from model, Tri=trilateration. Types of surface creep observations are listed as follows: I=interseismic creep, A=afterslip creep, T=transient or triggered creep.

Longitude	Latitude	Creep Rate (mm/yr)	Sigma (mm/yr)	Creep Type	Inst. Type	Start Date	End Date	Source
				Bartlett Springs Fault				
-122.9526	39.4539	8.2	2	I	Mod	1991	1995	Freymueller et al. (1999)
				Calaveras Fault				
-121.9598	37.7458	0.2	0.1	I	AA	1980	1989	Galehouse & Lienkaemper (2003)
-121.9359	37.7044	2.8	0.5	I	AA	1965	1977	Lisowski & Prescott (1981)
-121.8642	37.581	2.9	0.3	I	Geod	1965	1976	Prescott et al. (1981)

-121.8508	37.5358	3.6	0.5	I	AA	1997	2001	Galehouse & Lienkaemper (2003)
-121.812	37.4578	2.2	0.5	I	Geod	1970	1979	Prescott et al. (1981)
-121.7139	37.3417	9.4	0.4	I/A	Geod	1977	1984	Oppenheimer et al. (1990)
-121.5242	37.0699	14	2	I	AA	1968	1989	Galehouse & Lienkaemper (2003)
-121.4826	37.0096	13	2	I	Geod	1972	1979	Lisowski & Prescott (1981)
-121.4128	36.8699	13	Und	I/A	CM	1971	1983	Schulz (1982)
-121.4128	36.8496	12.2	0.2	I/A	AA	1979	1989	Galehouse & Lienkaemper (2003)
-121.4053	36.8496	6.4	0.2	I/A	AA	1979	1989	Galehouse & Lienkaemper (2003)
-121.3736	36.805	5	3	I	Geod	1975	1979	Lisowski & Prescott (1981)
-121.3233	36.805	6.2	0.1	I	AA	1973	1986	Wilmesher & Baker (1987)
-121.1425	36.5932	10	3	I	Geod	1975	1979	Lisowski & Prescott (1981)
Concord Fault								
-122.0372	37.9758	2.7	0.03	I	AA	1979	2001	Galehouse & Lienkaemper (2003)
-122.0342	37.972	3.6	0.04	I	AA	1979	2001	Galehouse & Lienkaemper (2003)
Garlock Fault								
-117.352	35.532	0	Und	I	AA	1971	1983	Louie et al. (1985)
-117.656	35.452	0	Und	I	AA	1971	1983	Louie et al. (1985)
-118.299	35.0898	5.7	1.5	I	AA	1971	1982	Louie et al. (1985)
Green Valley Fault								
-122.1495	38.1986	4.4	0.1	I	AA	1984	2001	Galehouse & Lienkaemper (2003)
Hayward Fault								
-122.3546	37.9891	5	0.1	I	AA	1968.33	1993.06	Lienkaemper et al. (2001)
-122.3379	37.969	4.8	0.2	I	AA	1980.61	1999.89	Lienkaemper et al. (2001)
-122.3083	37.9425	4.9	0.4	I	AA	1989.75	1999.68	Lienkaemper et al. (2001)
-122.2918	37.9246	4.4	0.3	I	AA	1989.75	1999.87	Lienkaemper et al. (2001)
-122.2506	37.8719	4.6	0.1	I	AA	1966.91	1999.66	Lienkaemper et al. (2001)
-122.2304	37.8484	3.8	0.1	I	AA	1974.26	1999.70	Lienkaemper et al. (2001)
-122.209	37.8264	3.7	0.2	I	AA	1993.11	1999.89	Lienkaemper et al. (2001)
-122.1975	37.8101	3.7	0.1	I	AA	1970.29	1999.70	Lienkaemper et al. (2001)
-122.1882	37.7951	3.6	0.3	I	AA	1974.27	1999.66	Lienkaemper et al. (2001)
-122.1504	37.7546	3.7	0.5	I	AA	1989.69	1999.89	Lienkaemper et al. (2001)
-122.1285	37.7319	5.9	0.5	I	AA	1993.39	1999.68	Lienkaemper et al. (2001)
-122.1045	37.695	5.5	0.9	I	AA	1992.62	1999.66	Lienkaemper et al. (2001)
-122.0899	37.6798	5	0.1	I	AA	1967.17	1999.83	Lienkaemper et al. (2001)
-122.0804	37.6703	4.4	0.1	I	AA	1980.48	1999.83	Lienkaemper et al. (2001)
-122.0727	37.6627	4	0.6	I	AA	1977.07	1999.68	Lienkaemper et al. (2001)
-122.0579	37.6481	6.7	0.5	I	AA	1994.59	1999.68	Lienkaemper et al. (2001)
-122.0222	37.6143	5.1	0.7	I	AA	1994.59	1999.70	Lienkaemper et al. (2001)
-122.0008	37.5925	5.1	0.2	I	AA	1979.73	1999.83	Lienkaemper et al. (2001)
-121.9797	37.5664	6	1.3	I	AA	1983.76	1988.85	Lienkaemper et al. (2001)
-121.9607	37.5422	5.6	0.3	I	AA	1979.73	1989.81	Lienkaemper et al. (2001)
-121.9548	37.5361	8.9	0.6	I	Cult	1940.3	1987.64	Lienkaemper et al. (2001)
-121.9343	37.5125	9.5	0.6	I	Cult	1967.7	1987.64	Lienkaemper et al. (2001)
-121.9316	37.5097	8.2	0.4	I	Cult	1968.7	1982.3	Lienkaemper et al. (2001)

Imperial Fault								
-115.51	32.862	13	8	I	AA	1974	1979	Louie et al. (1985)
-115.488	32.837	5.4	Und	I/T	AA	1967	1978	Louie et al. (1985)
-115.4787	32.8202	5	Und	I	CM	?	1979	Louie et al. (1985)
-115.356	32.683	1	Und	I	?	?	1977	Goulty et al. (1978)
-115.356	32.683	1.4	Und	I	CM	1975	1979	Louie et al. (1985)
-115.356	32.683	6	Und	A	CM	1980	1984	Louie et al. (1985)
Maacama Fault								
-123.3559	39.4125	6.5	0.1	I	AA	1991	2001	Galehouse & Lienkaemper (2003)
-123.1664	39.1392	4.4	0.2	I	AA	1993	2001	Galehouse & Lienkaemper (2003)
Rodgers Creek Fault								
-122.7083	38.4701	0.4	0.5	I	AA	1980	1986	Galehouse & Lienkaemper (2003)
-122.6405	38.3478	1.6	0.1	I	AA	1986	2000	Galehouse & Lienkaemper (2003)
-122.4469	38.0987	1.4	1.1	I	Tri	1978	1988	Lienkaemper et al. (1991)
San Andreas Fault								
-123.6895	39.0000	0.5	0.10	I	AA	1981	2000	Galehouse & Lienkaemper (2003)
-122.7969	38.0441	0.2	0.0	I	AA	1985	2001	Galehouse & Lienkaemper (2003)
-122.4646	37.6443	-0.3	0.02	I	AA	1980	1994	Galehouse & Lienkaemper (2003)
-122.2605	37.4171	0.3	0.1	I	AA	1989	2000	Galehouse & Lienkaemper (2003)
-121.6483	36.9267	0.8	0.4	I	AA	1967	1972	Burford & Harsh (1980)
-121.5851	36.8827	0.1	0.1	I	AA	1989	1998	Galehouse & Lienkaemper (2003)
-121.5453	36.8549	8	0.2	I	Cult	1942	1978	Burford & Harsh (1980)
-121.52	36.84	9	Und	I/T	CM	1969	1976	Burford (1988)
-121.5250	36.8392	13.3	0.2	I	Cult	1926	1978	Burford & Harsh (1980)
-121.5200	36.8367	14	0.4	I	AA	1968	1977	Burford & Harsh (1980)
-121.5207	36.8351	10.4	0.2	I	AA	1990	2001	Galehouse & Lienkaemper (2003)
-121.50	36.82	8.1	Und	I/T	CM	1969	1976	Burford (1988)
-121.42	36.77	10.9	Und	I/T	CM	1969	1976	Burford (1988)
-121.390	36.75	12.3	Und	I/T	CM	1958	1976	Burford (1988)
-121.3839	36.7495	12.3	0.2	I	Cult	1948	1976	Burford & Harsh (1980)
-121.3467	36.7200	13.5	0.4	I	AA	1972	1977	Burford & Harsh (1980)
-121.2717	36.6583	14	0.4	I	AA	1973	1977	Burford & Harsh (1980)
-121.23	36.65	13.8	Und	I/T	CM	1969	1976	Burford (1988)
-121.2017	36.6050	19.9	0.4	I	AA	1972	1977	Burford & Harsh (1980)
-121.19	36.6	20.3	Und	I/T	CM	1969	1976	Burford (1988)
-121.1943	36.5988	19	0.2	I	Cult	1937	1966	Brown & Wallace (1968)
-121.1850	36.5950	22.7	0.4	I	AA	1972	1977	Burford & Harsh (1980)
-121.1845	36.5933	22.9	0.4	I	AA	1967	1978	Burford & Harsh (1980)
-121.1841	36.5902	22	0.2	I	Cult	1945	1978	Burford & Harsh (1980)
-121.18	36.59	21.2	Und	I/T	CM	1969	1976	Burford (1988)
-121.1835	36.5740	23.1	0.4	I	AA	1970	1973	Burford & Harsh (1980)
-121.1630	36.5735	8	0.2	I	Cult	1951	1966	Brown & Wallace (1968)
-121.1350	36.5433	23.1	0.4	I	AA	1972	1977	Burford & Harsh (1980)
-121.0517	36.4817	21.9	0.4	I	AA	1967	1974	Burford & Harsh (1980)
-120.9823	36.3972	25	0.2	I	Cult	1908	1966	Brown & Wallace (1968)
-120.9750	36.3883	31.3	0.4	I	AA	1970	1976	Burford & Harsh (1980)

-120.969	36.3883	23.2	1	I	GPS	1967	2003	Titus et al. (2005)
-120.9693	36.3833	33.3	0.4	I	AA	1967	1971	Burford & Harsh (1980)
-120.9687	36.3828	28	0.2	I	Cult	1941	1966	Brown & Wallace (1968)
-120.9017	36.3167	31.4	0.4	I	AA	1970	1977	Burford & Harsh (1980)
-120.7983	36.2133	17.3	0.4	I	AA	1968	1977	Burford & Harsh (1980)
-120.7567	36.1800	26	0.4	I	AA	1970	1977	Burford & Harsh (1980)
-120.798	36.18	26.7	1	I	GPS	1970	2003	Titus et al. (2005)
-120.63	36.07	22.1	Und	I/T	CM	1972	1987	Burford (1988)
-120.6283	36.0650	30	0.4	I	AA	1968	1979	Burford & Harsh (1980)
-120.628	36.065	24.9	1	I	GPS	1968	2003	Titus et al. (2005)
-120.5717	36.0150	23.8	0.4	I	AA	1970	1979	Burford & Harsh (1980)
-120.5357	35.9837	25	0.2	I	Cult	1946	1966	Wallace & Roth (1967)
-120.4337	35.8951	22	0.2	I	Cult	1932	1978	Burford & Harsh (1980)
-120.4217	35.8850	14.6	0.4	I	AA	1968	1979	Burford & Harsh (1980)
-120.42	35.88	8.3	Und	I/T	CM	1972	1987	Burford (1988)
-120.36	35.84	3.97	Und	I/T	CM	1971	1987	Burford (1988)
-120.35	35.82	3.25	Und	I/T	CM	1972	1987	Burford (1988)
-120.3072	35.7567	18	0.2	I	Cult	1908	1978	Burford & Harsh (1980)
-120.3071	35.7566	4	0.4	I	AA	1966	1979	Burford & Harsh (1980)
-120.2267	35.6728	0	0.2	I	Cult	1937	1966	Brown & Wallace (1968)
-120.2050	35.6517	0	0.4	I	AA	1975	1977	Burford & Harsh (1980)
-118.11	34.55	0	0.5	I	AA	1970	1984	Louie et al. (1985)
-117.888	34.457	0	0.2	I	AA	1970	1984	Louie et al. (1985)
-117.8	34.422	0	1	I	AA	1970	1981	Louie et al. (1985)
-117.49	34.2858	0	0.5	I	AA	1970	1984	Louie et al. (1985)
-117.276	34.174	0	1	I	AA	1970	1983	Louie et al. (1985)
-116.964	34.058	0	0.4	I	AA	1970	1983	Louie et al. (1985)
-116.616	33.9325	2	Und	I	AA	1972	1982	Louie et al. (1985)
-116.234	33.777	1.5	0.6	I	AA	1970	1984	Louie et al. (1985)
-116.156	33.715	2	1	I/T	AA	1970	1984	Louie et al. (1985)
-115.99	33.58	1.7	Und	A	AA	1967	1983	Louie et al. (1985)
-115.949	33.541	0	0.1	I	CM	1970	1984	Louie et al. (1985)
-115.887	33.482	0.7	Und	I	CM	1981	1984	Louie et al. (1985)
				San Jacinto Fault				
-117.264	34.0442	0	1	I	AA	1973	1983	Louie et al. (1985)
-116.669	33.5861	0	2	I	AA	1977	1984	Louie et al. (1985)
-116.05	33.09	5.2	3	I/A	AA	1971	1984	Louie et al. (1985)
				Sargent Fault				
-121.6462	36.9763	2.9	0.7	I	Geod	1970	1975	Prescott & Burford (1976)
				Superstition Hills Fault				
-115.6633	32.9045	0.5	Und	I	CM	1968	1979	Louie et al. (1985)
				West Napa Fault				
-122.3393	38.3353	0.1	0.1	I	AA	1980	1999	Galehouse & Lienkaemper (2003)

Part Two: Line Integrals across the Pacific - North America plate boundary

To test the WG-07 source model, four line integrals were constructed across the underlying deformation model in California. We used the method of *Humphreys and Weldon* (1994) to accumulate uncertainty along the path, and used several input values, including uncertainties in the rake and orientation of the faults, deformation between stable North America and California (Figure P4), and block rotations, from *Humphreys and Weldon* (1994) where the WG-07 model does not contain the required data. Fault slip rates (Table P2 and P5) were taken from deformation model 2.1 (Appendix A); all other deformation models would produce similar results because they largely trade slip rate between the sub-parallel San Andreas and San Jacinto faults, and contain slightly different representations of the geometry of a few faults. The paths were chosen, from south to north, to cross the plate boundary 1) across the Salton Depression, Peninsular Ranges and Continental Borderland south of Los Angeles, 2) through the Mojave Desert and the Transverse Ranges just north of Los Angeles, 3) across the Eastern California Shear Zone, Sierra Nevada and Central California near Parkfield, and 4) through Northern California near the latitude of the Bay Area (Figure P5). Paths 1-3 repeat those of *Humphreys and Weldon* (1994) and yield very similar results. Deformation along all paths sum to values that overlap in uncertainty with the Pacific North America plate rate (Figure P6 and Table P2). While this appears to be a powerful vindication of the WG-07 model, it should not be too unexpected because past Working Group models, upon which this one is built, have been "tuned" to match the known plate rate, by choosing "preferred" values from a broad range of uncertain slip rates that approximately add up to the plate rate.

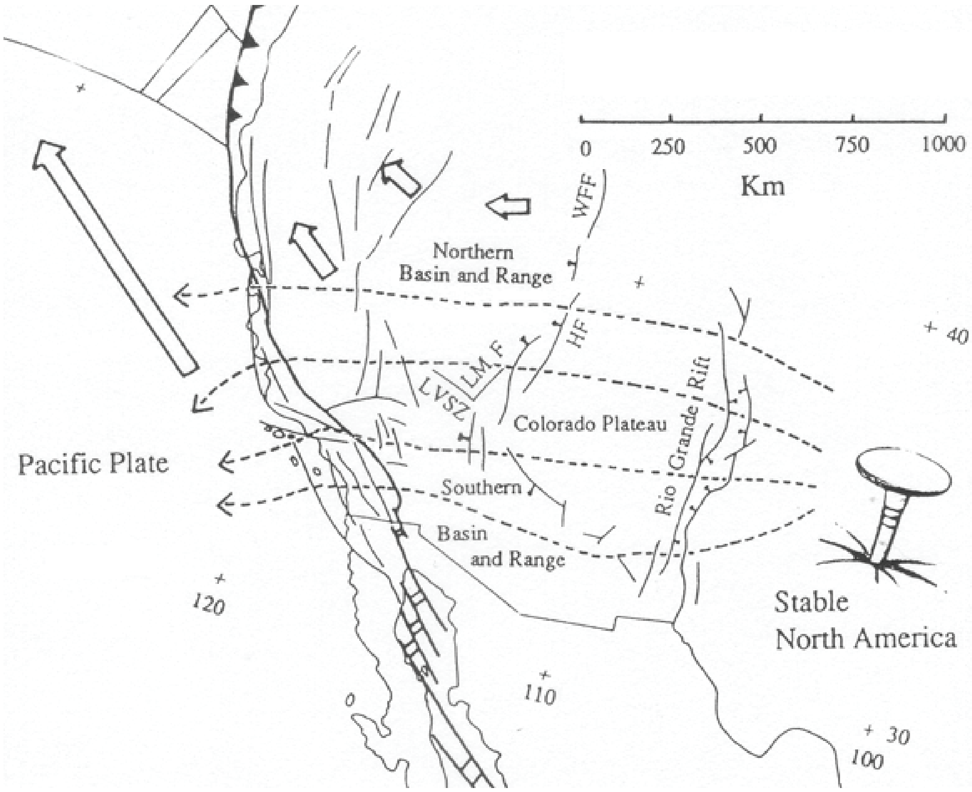

Figure P4 – Approximate location of line integrals across the Pacific – North America plate boundary; modified from *Humphreys and Weldon* (1994). Because the WG-07 model does not extend significantly east of California, we used the values for deformation east of California from *Humphreys and Weldon* (1994) to complete the paths between the Pacific and North American plates. Due to the influence of the Juan de Fuca subduction zone (bold teeth on NW edge of figure) no path was constructed for northernmost California.

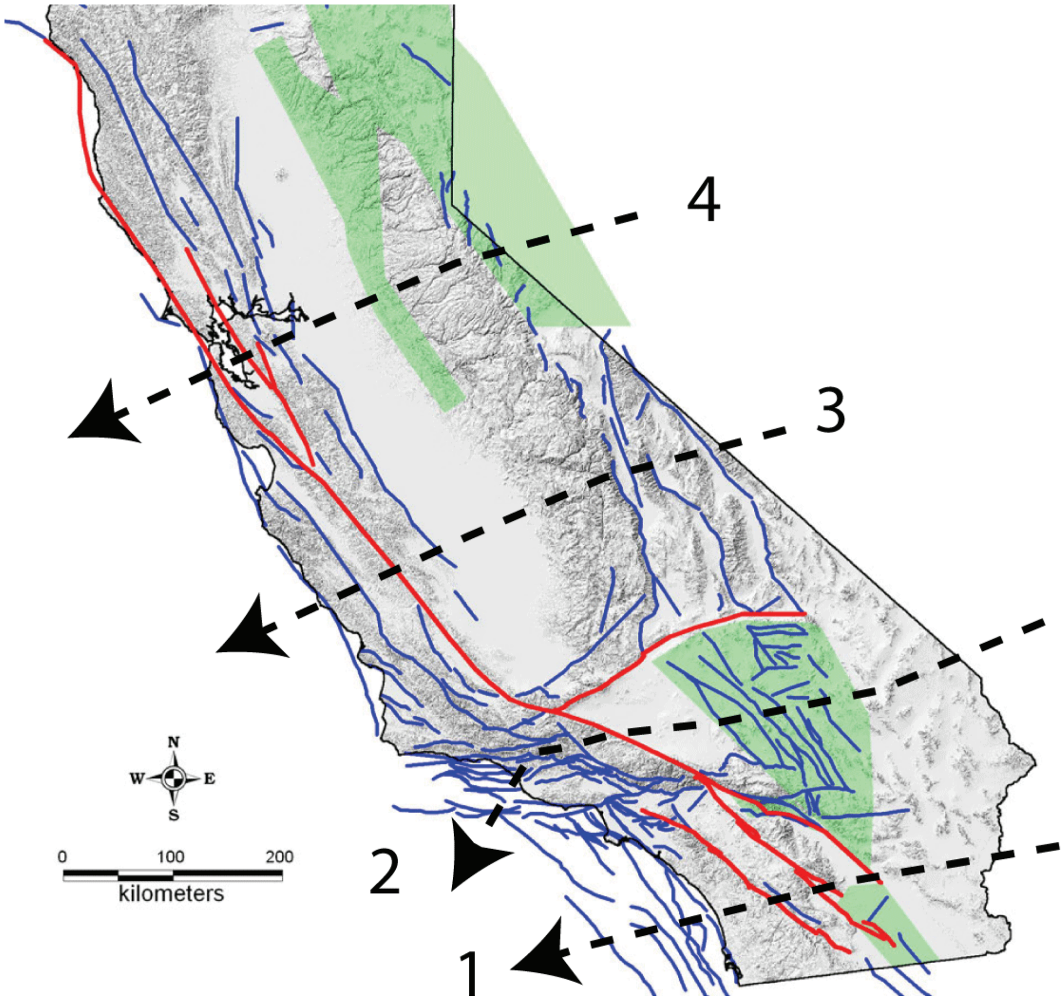

Figure P5 – Approximate location of line integrals 1) Peninsular Ranges path, 2) Transverse Ranges path, 3) Central California path, and 4) Northern California path. Deformation east of the modeled area is included from *Humphreys and Weldon* (1994). Red lines are A-Faults, blue B-Faults, and green polygons are C-zones, which are modeled as vertical faults with simple shear appropriately oriented. Faults and C-zones included in each path are listed in Table P2.

Line integrals are very sensitive to the path chosen. As can be seen in Figure P5, it is easy to change slightly the path to avoid or add discontinuous structures or cross longer faults where the geometry, slip rate, dip or rake vary. Thus, the uncertainties reflected in Figure P6 and Table P2 should be considered minimums that do not take into account possible different paths. One could test possible differences between closely spaced paths, by a Monte Carlo sampling approach, like that used by *Humphreys and Weldon* (1994) to determine cumulative uncertainty in each path. This was not done but it is clear from qualitative examination of the data that only the Transverse Ranges path would change by more than a few millimeters per year. In addition, line integral paths that cross rotating blocks must correctly account for rotations that are not explicitly included in our deformation model. We have used the rotations determined by *Humphreys and Weldon* (1994), but it is unlikely, particularly in southern California, that all of the rotations are known and well characterized. This may be the reason for the systematic more westerly direction we determine for all three southern paths and the slight underestimate in rate for the most complex Transverse Ranges path, which crosses multiple, rapidly rotating blocks.

Table P2: Inputs and Summary of Line Integral Analysis

Path	Faults and C-zones included (1)	Best Estimate Rate (mm/yr) (2)	Best Estimate Direction (NW) (2)	Vector Sum Rate (3) (mm/yr)	Vector Sum Direction (NW) (3)	Plate Rate (mm/yr) & Direction (NW) (4)
Peninsular Range	97,113,114,115,171,172	48.2±7.9	47.1±3.8°	49.8	46.6°	47.6/41.4°
Transverse Range	76,80,81,84,85,86,104, 108,109,158,178,187	38.9±7.4	45.6±10.7°	38.5	48.1°	47.5/38.3°
Central California	10,30,32,59,60,83, 130,134,155,156	46.9±5.4	40.5±5.2°	48.1	41.0°	47.7/35.5°
Northern California	2,4,7,12,39,44,63, 65,125,183,186	52.0±7.9	32.5±3.4°	52.3	32.9°	47.3/32.1°

1) Numbers refer to faults listed in Table P5; strike, dip, rake and slip rate for each fault and C-zone are found in the second half of Table P5. Additional information including block rotations and uncertainties in fault geometry and rake of slip for most faults are from *Humphreys and Weldon* (1994; Table 1, p. 19,981). Uncertainties in geometry and rake of slip for faults not included in *Humphreys and Weldon* (1994) are assumed to have the average uncertainty of those modeled.
2) 90% confidence limits, following *Humphreys and Weldon* (1994).
3) The vector sum differs from the best estimate due to asymmetries in the cumulative uncertainties generated by adding nonparallel vectors.
4) NUVEL-1A (*DeMets, et al.,* 1994). Pacific plate motion relative to North America calculated at path ends.

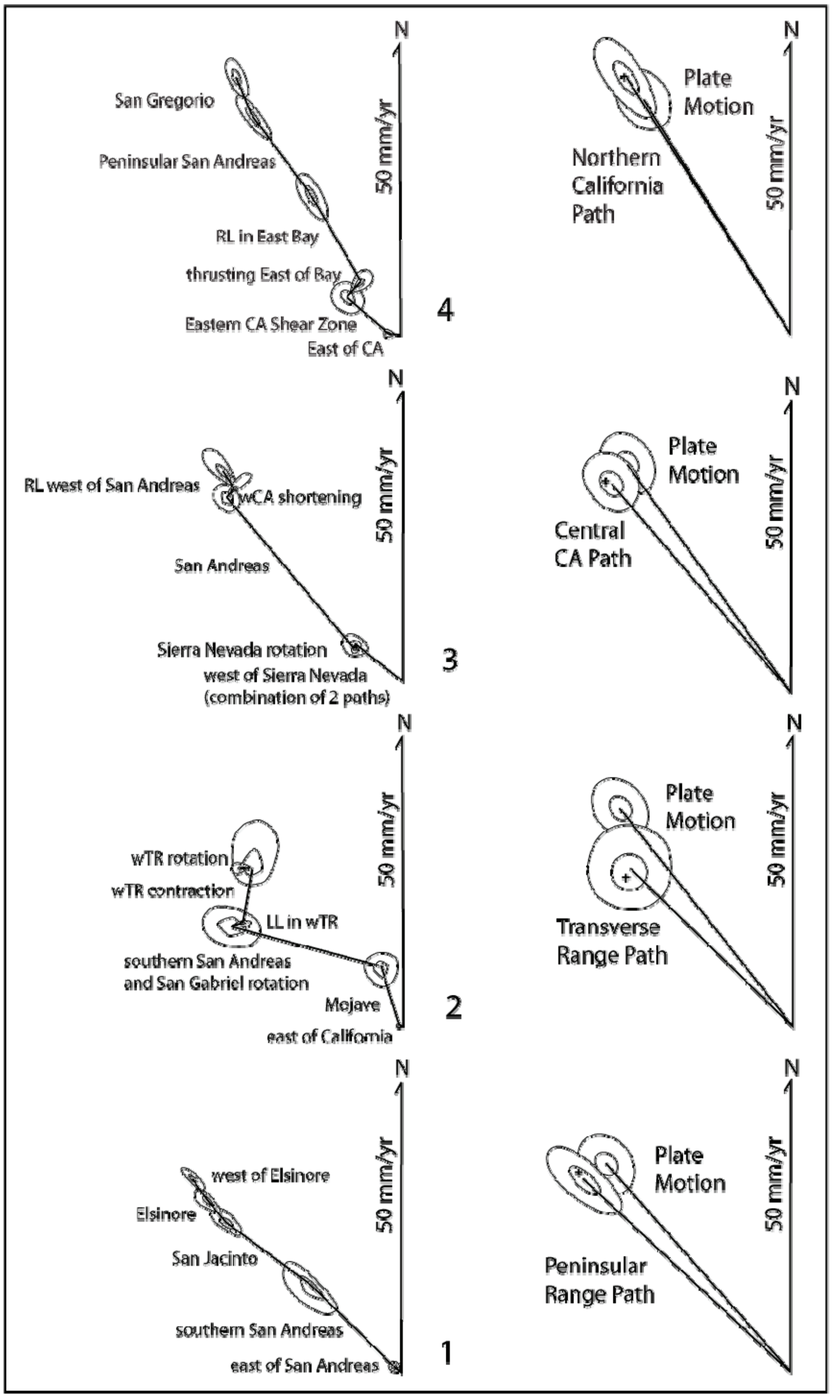

Figure P6 – Vector sum of line integrals compared to the expected Pacific North America plate motion. The tip of the vectors are the best estimate from Monte Carlo sampling of the uncertainties associated with all inputs and the uncertainty contours are 30 and 90% (following *Humphreys and Weldon,* 1994; which used 30, 60 and 90% - the 60% range is left off here for clarity). The pluses are the sum of the individual fault slip vectors (and rotations), and are distinct from the best estimates because the individual fault uncertainties are quite asymmetric. Note the plate motion varies slightly from path to path, becoming more northerly to the north.

WG-07 does not include a number of inputs that are required to construct line integrals and to estimate their uncertainty. First, WG-07 does not include any information about the deformation beyond a narrow buffer zone east of California. To complete the analysis we used the values from *Humphreys and Weldon* (1994) for the southern 3 paths and used the same rate of extension across the northern Basin and Range from path 3 for the northernmost path (4). Second, there are no rotations explicitly included in WG-07. Integrating along paths that cross rotating blocks accumulates deformation associated with the rotation, so must be explicitly included in the analysis. To do so we used the rotations estimated by *Humphreys and Weldon* (1994). Finally, the WG-07 model does not contain estimates of uncertainty in strike, dip, or rake of faults. Again, we used the uncertainties from *Weldon and Humphreys* (1994) for faults that they considered and added uncertainties with similar ranges to those faults they did not consider. To estimate how uncertainties accumulate along the path of the line integral, we used the *Humphreys and Weldon* (1994) approach of Monte Carlo sampling the uncertainties of individual faults that the path includes. An analytical approach was not possible because many of the uncertainties are highly asymmetrical. The results of this uncertainty analysis are represented by uncertainty ellipses that approximate uncertainty thresholds in the final results (Figure P6). Simple vector sums of the inputs are also included for comparison (Table P2).

At least 2 of the paths (Northern California and Peninsular Ranges) appear to accumulate slightly more deformation than the plate rate (Figure P6, Table P2). This is surprising given that the line integrals do not include distributed deformation (represented in WG-07 model as "background" seismicity). This is in contrast to our strain tensors (discussed in Part 3), which explicitly include background seismicity, yet generally yield just under the plate rate. The answer to this possible discrepancy (it is all within reasonable uncertainties, so may not be significant) is that the line integrals are generally chosen to cross the faults where the slip rates are best known and the faults are simple, straight, and generally parallel to the plate boundary (except for the Transverse Ranges path, which has the lowest total rate; Figure P6, Table P2). In contrast, the strain tensors combine deformation in large crustal volumes, so include both regions where simple and complex faults occur and, in discontinuous fault zones, the gaps in between. It is possible that by choosing the "best" paths and slip rates we are biasing the result towards higher slip rates that may not be representative of the fault as a whole. This is especially true for discontinuous zones where the slip rate used often comes from the middle of a fault where the slip rate is the highest and the actual slip rate tapers to each end of individual strands. A line integral could cross the fault in the middle, where the rate is high, whereas the strain tensor would include the gaps (and tapered ends, if they have lower slip rates) in between as well.

It is also possible that the actual plate rate is higher than the widely accepted long term rate (~48 mm/yr, NUVEL-1A, *DeMets et al., 1994,* shown on Figure P6); recent GPS and VLBI studies suggest the decadal rate may be 5-10% higher (e.g. *Wdowinski et al.,* 2007). If this is the case, then picking paths along simple, well studied paths may yield values that approach the real plate rate, whereas the volumes considered in the strain tensor approach would slightly underestimate the instantaneous plate rate because it includes regions where the deformation is expressed in a few simple faults and others where it is more distributed and thus more difficult to capture in a simple model.

Part Three - Strain Tensor Analysis

To test WG-07 deformation and seismic source models, we have constructed strain tensors across the Pacific - North American plate boundary and compared them to predictions from the far field plate motion. We used the Kostrov (1974) method as presented in Aki and Richards (1984). Molnar (1983; 1979; et al., 2007; Chen and Molnar, 1977) and many others have discussed the relative merits of using symmetrical strain tensors (as we do) versus asymmetrical tensors or a combination of rotational and irrotational components of the deformation field. We finesse this issue to some extent by comparing principal strain axes from our symmetrical strain tensors to those resulting from a single ideally-oriented (plate boundary parallel) fault, with the plate rate of slip, embedded in the same volume as the distributed deformation we consider. The fact that the distributed deformation almost exactly equals the strain inferred from the Pacific - North America plate motion in both rate and style suggest that symmetrical tensors adequately capture the deformation. We have analyzed ten 3D volumes spanning our model, oriented perpendicular to the plate boundary (Figure P7; results summarized in Table P3). We have cut off northernmost California north of the Mendocino triple junction because of the possible influence of the Juan de Fuca subduction zone. We also limited the southern end of the model to approximately the US Mexico border because the coverage of faults drops into Mexico and there are no C- zones south of the US border (Figure P5). Faults that cross box boundaries are weighted by the fraction of the fault in the box (see Table P5).

For each block we calculate a strain tensor for both deformation and seismic source models. This distinction is important because the deformation model includes the full slip rates on the faults and C-zones, plus an estimate of distributed seismicity that is inferred to represent deformation between modeled faults. Because the structures associated with distributed seismicity are unknown, we assume that they have, on average, the same geometry as the larger faults in the volume being considered. In contrast to the deformation model, the WG-07 seismic source model reduces the moment (and thus strain) associated with each fault by a fixed amount (10%) to account for aftershocks, post seismic slip, possible aseismic permanent deformation along fault zones and other processes that are part of the deformation model but not the source model. In addition, moment is reduced for faults that creep, and there are no aftershocks in the model. While the deformation model can be compared directly to the plate motion, the source model cannot, due to these reductions, but it can be compared to the macroseismic component of slip across similar plate boundaries (e.g. Bird and Kagan, 2004) or to see if the fraction of strain released as modeled earthquakes varies across different parts of California. To compare the strain tensors to the strain associated with the plate motion (and each other) we calculate principal strain axes and their directions from the eigenvalues and eigenvectors of the tensors, and compare them to the principal strains from a single, simple plate boundary parallel fault embedded in the same volume. In addition to being an easy way to compare tensors, this reduces the impact of model assumptions like the block depths, rigidity, etc.

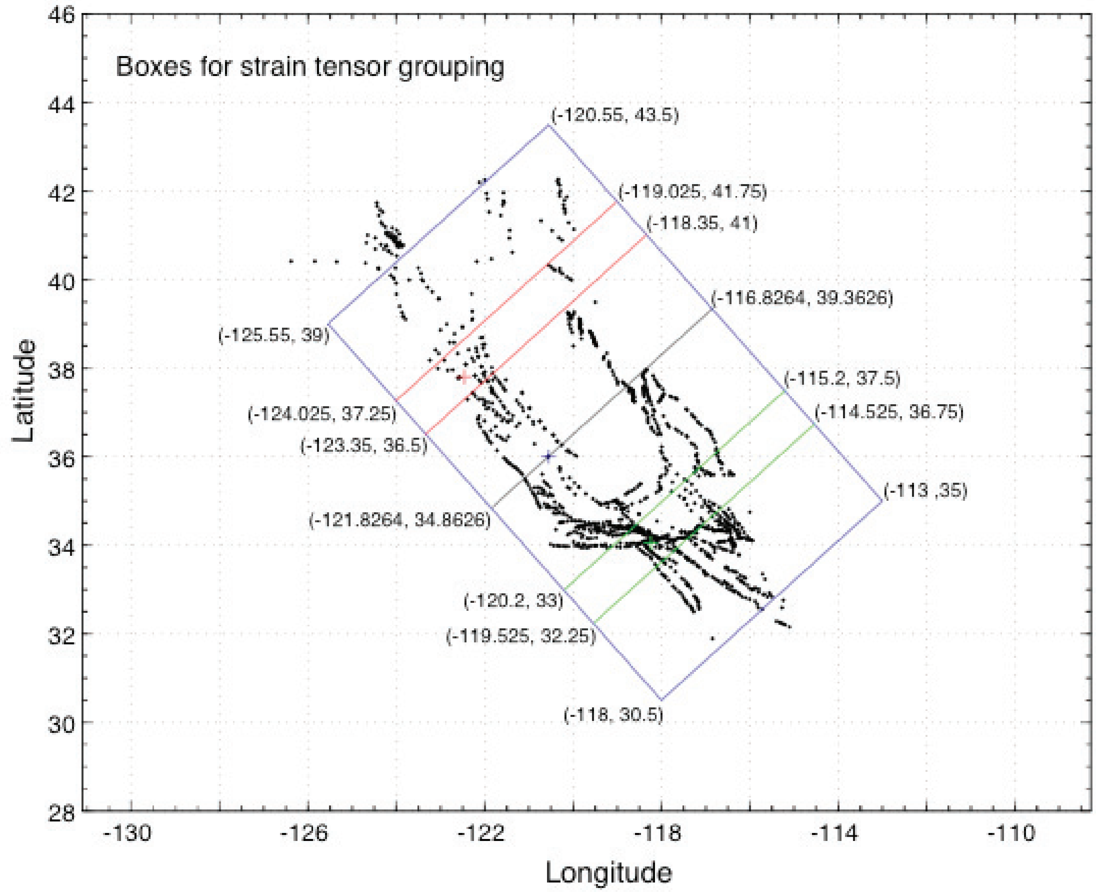

Figure P7 – Volumes considered for strain tensor analysis (the thickness (depth) of each volume is the average depth of the faults in the volume, included in Table P4). Black dots are the ends points of individual linear portions of faults or fault sections. Blue box is the "entire" region considered (it is smaller than the WG-07 model because we limited it at the Mendocino triple junction and the Mexican border). Black line separates the northern and southern volumes, divided at the southern end of the Creeping section of the San Andreas fault (blue +). Red and green are the San Francisco and Los Angeles regions, respectively.

For each block we calculate a strain tensor for both deformation and seismic source models. This distinction is important because the deformation model includes the full slip rates on the faults and C-zones, plus an estimate of distributed seismicity that is inferred to represent deformation between modeled faults. Because the structures associated with distributed seismicity are unknown, we assume that they have, on average, the same geometry as the larger faults in the volume being considered. In contrast to the deformation model, the WG-07 seismic source model reduces the moment (and thus strain) associated with each fault by a fixed amount (10%) to account for aftershocks, post seismic slip, possible aseismic permanent deformation along fault zones and other processes that are part of the deformation model but not the source model. In addition, moment is reduced for faults that creep, and there are no aftershocks in the model. While the deformation model can be compared directly to the plate motion, the source model cannot, due to these reductions, but it can be compared to the macroseismic component of slip across similar plate boundaries (e.g. Bird and Kagan, 2004) or to see if the fraction of strain released as modeled earthquakes varies across different parts of California. To compare the strain tensors to the strain associated with the plate motion (and each other) we calculate principal strain axes and their directions from the eigenvalues and eigenvectors of the tensors, and compare them to the principal strains from a single, simple plate boundary parallel fault embedded in the same volume. In addition to being an easy way to compare tensors, this reduces the impact of model assumptions like the block depths, rigidity, etc.

For the entire region, WG-07 deformation model accounts for ~95% of the plate motion (summarized in Table P3; tensors are in Table P4, and input values are found in Table P5). This is almost certainly within the calculation uncertainty, which includes the slip rates on the faults, the rate of background seismicity and aftershocks, the depths of the faults and the thickness of the block being deformed. If significant, the small additional 5% of strain generated by the plate motion may be aseismic strain that is off our modeled faults (Aseismic strain on the faults would be included in the fault's slip rate, and thus in our deformation model; however, for unmodeled faults, i.e. our "background," we can only "account" for the seismically observed component). Alternatively, we may have incompletely estimated the "background" rate of deformation because it does not formally include aftershocks.

Table P3: Summary of Stain tensor Analysis

Block	**Deformation Model**			**Source Model**		
	Percent Accommodated By Model (1)	Angular Difference (2)	Vertical Change (3)	Percent Accommodated By Model (1)	Angular Difference (2)	Vertical Change (3)
Entire Region	90.8%	-5.9°	3.8%	64.6%	-6.7°	3.5%
North 1/2	95.9% (4)	-3.0°	-1.6%	56.7%	-1.3°	-1.6%
South 1/2	95.2% (4)	-10.2°	8.6%	78.4%	-10.7°	7.9%
San Francisco	90.9%	-2.3°	1.9%	67.1%	-1.9°	1.9%
North of San Francisco	97.8%	1.1°	-2.8%	68.0%	1.8°	-2.5%
Los Angeles	101.0%	-13.5°	16.5%	84.4%	-12.6°	14.9%
South of Los Angeles	85.7% (5)	-5.5°	0.6%	68.8% (5)	-6.8°	0.6%

1) Percentage of Pacific – North America plate motion accommodated by the model (calculated as the ratio of the maximum principal strain axes presented in Table P4).
2) Angular difference between the orientation of principal strain axes of the model and average Pacific – North America plate motion; positive is more northerly and negative more westerly.
3) Percentage of thickening (positive) or thinning (negative) of the block relative to the simple shear component (ideal Pacific – North America plate motion has only simple shear and thus no block thickening or thinning).
4) These values do not average to the State total because each box is calculated with the average depth of all of the faults in the box. If one fixes the thickness of the boxes to the State average (~13 km) one would calculate 88.7% for the northern, and 98.7% for the southern. Since the average depth of faulting is a real difference between northern and southern California it is more appropriate to use the different average depths of each to compare to the plate boundary total.
5) This value is very sensitive to the rate and orientation of shear applied to the Imperial C-zone and the spatial cut off of the block being considered (since the density of mapped faults drops dramatically into Mexico). An early calculation using the Imperial C-zone of Rate Model 2.2 and a slightly different spatial cut off yielded 115%. Because the Imperial C-zone contributes no seismicity beyond the background rate in the current source model, the percent of shear in the source model is as accurate as other boxes.

For the entire region, our seismic source model accounts for ~70% (64.6% plus an estimated 5% aftershocks that are not included in the model) of the plate motion. This is very consistent with the global average seismic component of strike slip plate boundaries (*Bird and Kagan,* 2004).

To explore the differences between northern and southern California we split the region approximately in half, perpendicular to the plate boundary, through the northern end of the Parkfield section of the San Andreas fault (or southern end of the Creeping section). The deformation model yields 95.9% for the northern half of the State and 95.2% for the southern. The apparent discrepancy with the entire region (90.8%) is due to different block thicknesses for the different parts of the State. We use the average depth of all the faults in each block being considered to define the block thickness. For the entire State this is 13.0 km, whereas for Northern CA it is 12.0 km and for Southern CA it is 13.5 km (note that the results for the entire State is not the average of the two blocks because there are many more faults in the Southern California block). If one were to use the 13.0 average depth for the entire State the Northern California part of our model would have 88.7% and southern California 98.7% of the plate rate; however, since the difference in average depth of faulting is likely to be real, the ~95% values for each half of the State are probably correct.

The similarity of these values to each other and the plate rate strongly suggests that our model accurately captures the strain driving deformation across the plate boundary. In addition, the direction of calculated principal strain axes and small fraction of thickening of the boxes is consistent with the transform plate margin (Table P3).

The seismic components for Northern and Southern California are 56.7% and 78.4% respectively. This difference is almost certainly significant and is due to the fact that the Northern California block contains the Creeping section of the San Andreas fault, major faults in the Bay Area that have significant aseismicity factors and the large Eastern CA C-zone in which only 50% of the strain is seismic. In addition, the Southern CA block has many more B faults that are reverse in style, which due to their low dip and lack of aseismicity contribute significantly to the seismic component of the strain. Thus, the difference between Northern and Southern California probably represent real differences in the seismic component of the strain release across the plate boundary and not a bias in the model.

This real distinction between Southern and Northern California suggests that drawing conclusions from blocks smaller than the entire State may be dangerous. However, to explore possible regional differences we also consider ~100 km wide boxes centered on the San Francisco and Los Angeles regions and similar-sized boxes to the north and south.

The San Francisco block yields a deformation strain rate of 90.9% of the plate total and a seismic rate of 67.1% of the plate rate, essentially identical with the entire State. The block to the north of San Francisco gives slightly higher results of 92.7% and 65.0% respectively. We also looked at the western halves of these blocks (essentially the San Andreas system) and found no significant differences between the Bay Area and the region to the north (early calculations suggesting a difference were biased by errors in the dimensions and shear directions of the C-zones in an early version of the Rate Model).

The Los Angeles block yields a deformation strain rate of 101.0% of the plate total and a seismic rate of 84.4% of the plate rate. These values are 5-10% higher than elsewhere and may indicate real differences in the LA region, a slight bias in the data, or that the block is too small to accurately represent the plate rate. This block contains no known creeping faults, a relatively low slip rate C-zone (Mojave), and a large number of thrusts, so the slightly higher values may reflect a real regional difference.

If the LA rate is too high, it is likely to be because the LA region has a relatively large number of B faults that as a group may have slightly over-estimated slip rates. Finally, it is possible that a slight excess in strain in this block may be balanced by a deficit elsewhere. For example, *Humphreys and Weldon* (1994) have argued that the loss of surface area along the transform boundary from compression in the Transverse Ranges (largely included within the LA block) is balanced by creation of surface area in the Salton Depression and, potentially Eastern California. So it may simply require a larger region than the LA block to exactly account for the plate deformation.

The southernmost block, between LA and the Mexican border, yields a deformation strain rate of 85.7% of the plate total and a seismic rate of 68.8% of the plate rate. While the deformation rate may be lower than other blocks, the value is very sensitive to where the boundary is drawn (since the distribution of known faults drops rapidly to the south) and the rate assigned to the Imperial Valley C-zone. Earlier estimates using the higher rate on the Imperial C-zone in an earlier Rate Model and a slightly different spatial cut-off yielded a deformation strain rate of ~115% of the plate rate. The seismic rate, that approximately matches the State average value, is less sensitive to the border cut-off because the Imperial C-zone is modeled as being completely aseismic, so its rate does not affect the seismic source model at all.

Table P4 – Strain tensors for volumes shown in Figure P7

All faults are rotated to match the plate boundary strike for that region.

M is the moment tensor for simple single fault boxes.
SR is the strain rate matrix for simple single fault boxes.
V columns are the eigenvectors for **D** (eigenvalues for SR and M).
MsumS is the summed Moment tensor for each grouping of faults with a 10% increase from background seismicity (dyne·km).
MsumA is summed Moment tensor for each grouping of faults with a 10% increase from background seismicity, and a 10% decrease in moment, and incorporates an aseismicity factor.
SRS is the strain rate matrix including background seismicity (yr^{-1}).
SRA is the strain rate matrix including background seismicity and decreased moments and aseismicity factor.
Vs columns are the eigenvectors for **Ds** (eigenvalues for SRS and MsumS).
Va columns are the eigenvectors for **Da** (eigenvalues for SRA and MsumA).

EQUATIONS (from *Aki and Richards*, 1980)

$\mu = 3.3e+21$ dyne/km^2
$M_o \approx \mu As$
Where $\mu = 3.3e+21$ dyne/km^2
A = rupture area
s = slip

Δ = dip
Γ = rake
S = strike

$$M_{xx} = -M_o ((\sin \Delta \cos \Gamma \sin 2S) + (\sin 2\Delta \sin \Gamma \sin^2 S))$$

$$M_{xy} = M_o ((\sin \Delta \cos \Gamma \cos 2S) + (0.5*\sin 2\Delta \sin \Gamma \sin 2S)) = M_{yx}$$

$$M_{xz} = -M_o ((\cos \Delta \cos \Gamma \cos S) + (\cos 2\Delta \sin \Gamma \sin S)) = M_{zx}$$

$$M_{yy} = M_o ((\sin \Delta \cos \Gamma \sin 2S) - (\sin 2\Delta \sin \Gamma \cos^2 S))$$

$$M_{yz} = -M_o ((\cos \Delta \cos \Gamma \sin S) – (\cos 2\Delta \sin \Gamma \cos S)) = M_{zy}$$

$$M_{zz} = M_o (\sin 2\Delta \sin \Gamma)$$

$$\dot{\varepsilon} \cong (1/2\mu VT)\sum_{n=1}^{N} M_{ij}$$

Entire Block
Strike: Calculated using a plate boundary strike of N36°W
Dip: Vertical
Rake: 180 (right lateral)
Fault Surface Area: 16526.9 km^2
Slip Rate: 47 mm/yr
Depth = 13.0 km
Block volume: 1.2294e+7 km^3

M =

1.0e+27 *

0.5329	-2.5073	0
-2.5073	-0.5329	0
0	0	0

SR =

0.0066	-0.0309	0
-0.0309	-0.0066	0
0	0	0

V =

-0.6293	0	-0.7771
-0.7771	0	0.6293
0	1.0000	0

D =

-0.0316	0	0
0	0	0
0	0	0.0316

MsumS =

1.0e+27 *

-0.0395	-2.2799	0.0436
-2.2799	-0.0579	-0.0029
0.0436	-0.0029	0.0974

SRS =

-0.0005	-0.0281	0.0005
-0.0281	-0.0007	-0.0000
0.0005	-0.0000	0.0012

Vs =

0.7057	-0.0026	0.7085
0.7084	0.0193	-0.7055
-0.0118	0.9998	0.0154

Ds =

-0.0287	0	0
0	0.0012	0
0	0	0.0275

MsumA =

1.0e+27 *

-0.0809	-1.6119	0.0386
-1.6119	-0.0069	-0.0030
0.0386	-0.0030	0.0878

SRA =

-0.0010	-0.0199	0.0005
-0.0199	-0.0001	-0.0000
0.0005	-0.0000	0.0011

Va =

0.7152	-0.0033	0.6989
0.6988	0.0243	-0.7149
-0.0146	0.9997	0.0197

Da =

-0.0204	0	0
0	0.0011	0
0	0	0.0193

North Block
Strike: Calculated using a plate boundary strike of N32°W
Dip: Vertical
Rake: 180 (right lateral)
Fault Surface Area: 7542 km^2
Slip Rate: 47 mm/yr
Depth: 12.0 km
Block volume: 5.5561e+6 km^3

M =

1.0e+27 *

0.4001	-1.0992	0
-1.0992	-0.4001	0
0	0	0

MsumS =

1.0e+27 *

0.2808	-1.0789	0.0020
-1.0789	-0.2609	-0.0124
0.0020	-0.0124	-0.0199

MsumA

1.0e+26 *

2.0535	-6.2500	0.0164
-6.2500	-1.8764	-0.1152
0.0164	-0.1152	-0.1771

SR =

0.0109	-0.0300	0
-0.0300	-0.0109	0
0	0	0

SRS =

0.0077	-0.0294	0.0001
-0.0294	-0.0071	-0.0003
0.0001	-0.0003	-0.0005

SRA =

0.0056	-0.0170	0.0000
-0.0170	-0.0051	-0.0003
0.0000	-0.0003	-0.0005

V =

-0.5736	0	-0.8192
-0.8192	0	0.5736
0	1.0000	0

Vs =

0.6150	-0.0112	-0.7885
0.7885	-0.0013	0.6150
0.0079	0.9999	-0.0081

Va =

0.5915	-0.0175	-0.8061
0.8062	-0.0036	0.5917
0.0132	0.9998	-0.0119

D =

-0.0319	0	0
0	0	0
0	0	0.0319

Ds =

-0.0301	0	0
0	-0.0005	0
0	0	0.0306

Da =

-0.0176	0	0
0	-0.0005	0
0	0	0.0181

South Block

Strike: Calculated using a plate boundary strike of N38°W
Dip: Vertical
Rake: 180 (right lateral)
Fault Surface Area: 8733.2 km^2
Slip Rate: 47 mm/yr
Depth: 13.5 km
Block volume: 6.5162e+6 km^3

M =

1.0e+27 *

0.1885	-1.3413	0
-1.3413	-0.1885	0
0	0	0

SR =

0.0044	-0.0312	0
-0.0312	-0.0044	0
0	0	0

V =

-0.6561	0	-0.7547
-0.7547	0	0.6561
0	1.0000	0

D =

-0.0315	0	0
0	0	0
0	0	0.0315

MsumS =

1.0e+27 *

-0.3202	-1.2009	0.0416
-1.2009	0.2030	0.0095
0.0416	0.0095	0.1172

SRS =

-0.0074	-0.0279	0.0010
-0.0279	0.0047	0.0002
0.0010	0.0002	0.0027

Vs =

-0.7786	0.0101	-0.6275
-0.6270	0.0309	0.7784
0.0273	0.9995	-0.0177

Ds =

-0.0300	0	0
0	0.0027	0
0	0	0.0272

MsumA =

1.0e+26 *

-2.8807	-9.8225	0.3613
-9.8225	1.8256	0.0837
0.3613	0.0837	1.0551

SRA =

-0.0067	-0.0228	0.0008
-0.0228	0.0042	0.0002
0.0008	0.0002	0.0025

Va =

-0.7850	0.0110	-0.6194
-0.6189	0.0323	0.7848
0.0287	0.9994	-0.0186

Da =

-0.0247	0	0
0	0.0025	0
0	0	0.0223

<u>San Francisco Block</u>

Strike: Calculated using a plate boundary strike of N32°W
Dip: Vertical
Rake: 180 (right lateral)
Fault Surface Area: 1503.5 km^2
Slip Rate: 47 mm/yr
Depth: 13.2 km
Block volume: 1.1078e+6 km^3

M =

1.0e+26 *

0.7976	-2.1913	0
-2.1913	-0.7976	0
0	0	0

SR =

0.0109	-0.0300	0
-0.0300	-0.0109	0
0	0	0

V =

-0.5736	0	-0.8192
-0.8192	0	0.5736
0	1.0000	0

D =

-0.0319	0	0
0	0	0
0	0	0.0319

MsumS =

1.0e+26 *

0.5324	-2.0196	0.0139
-2.0196	-0.5788	-0.0316
0.0139	-0.0316	0.0464

SRS =

0.0073	-0.0276	0.0002
-0.0276	-0.0079	-0.0004
0.0002	-0.0004	0.0006

Vs =

0.6061	-0.0165	0.7953
0.7954	0.0029	-0.6061
0.0077	0.9999	0.0149

Ds =

-0.0290	0	0
0	0.0006	0
0	0	0.0283

MsumA =

1.0e+26 *

0.4122	-1.4848	0.0123
-1.4848	-0.4543	-0.0291
0.0123	-0.0291	0.0421

SRA =

0.0056	-0.0203	0.0002
-0.0203	-0.0062	-0.0004
0.0002	-0.0004	0.0006

Va =

0.5998	-0.0206	0.7998
0.8001	0.0031	-0.5999
0.0099	0.9998	0.0184

Da =

-0.0214	0	0
0	0.0006	0
0	0	0.0209

North of San Francisco Block
Strike: Calculated using a plate boundary strike of N32°W
Dip: Vertical
Rake: 180 (right lateral)
Fault Surface Area: 3040.4 km^2
Slip Rate: 47 mm/yr
Depth: 11.6 km
Block volume: 2.2395e+6 km^3

M =

1.0e+26 *

1.6129	-4.4313	0
-4.4313	-1.6129	0
0	0	0

MsumS =

1.0e+26 *

1.7808	-4.2117	-0.0005
-4.2117	-1.6516	-0.0195
-0.0005	-0.0195	-0.1293

MsumA =

1.0e+26 *

1.3199	-2.8897	-0.0005
-2.8897	-1.2036	-0.0175
-0.0005	-0.0175	-0.1163

SR =

0.0109	-0.0300	0
-0.0300	-0.0109	0
0	0	0

SRS =

0.0120	-0.0285	-0.0000
-0.0285	-0.0112	-0.0001
-0.0000	-0.0001	-0.0009

SRA =

0.0089	-0.0196	-0.0000
-0.0196	-0.0081	-0.0001
-0.0000	-0.0001	-0.0008

V =

-0.5736	0	-0.8192
-0.8192	0	0.5736
0	1.0000	0

Vs =

0.5580	-0.0039	-0.8299
0.8299	-0.0019	0.5580
0.0038	1.0000	-0.0022

Va =

0.5476	-0.0051	-0.8367
0.8367	-0.0027	0.5477
0.0050	1.0000	-0.0028

D =

-0.0319	0	0
0	0	0
0	0	0.0319

Ds =

-0.0303	0	0
0	-0.0009	0
0	0	0.0312

Da =

-0.0209	0	0
0	-0.0008	0
0	0	0.0217

Los Angeles Block
Strike: Strike: Calculated using a plate boundary strike of N38°W
Dip: Vertical
Rake: 180 (right lateral)
Fault Surface Area: 1541.3 km^2
Slip Rate: 47 mm/yr
Depth: 13.7 km
Block volume: 1.1498e+6 km^3

M =

1.0e+26 *

0.3327	-2.3673	0
-2.3673	-0.3327	0
0	0	0

SR =

0.0044	-0.0312	0
-0.0312	-0.0044	0
0	0	0

V =

-0.6561	0	-0.7547
-0.7547	0	0.6561
0	1.0000	0

D =

-0.0315	0	0
0	0	0
0	0	0.0315

MsumS =

1.0e+26 *

-0.9139	-2.0952	-0.0925
-2.0952	0.5232	-0.0275
-0.0925	-0.0275	0.3907

SRS =

-0.0120	-0.0276	-0.0012
-0.0276	0.0069	-0.0004
-0.0012	-0.0004	0.0051

Vs =

-0.8135	-0.0152	-0.5814
-0.5807	-0.0346	0.8134
-0.0325	0.9993	0.0193

Ds =

-0.0318	0	0
0	0.0052	0
0	0	0.0266

MsumA =

1.0e+26 *

-0.7203	-1.7544	-0.0832
-1.7544	0.3686	-0.0247
-0.0832	-0.0247	0.3517

SRA =

-0.0095	-0.0231	-0.0011
-0.0231	0.0049	-0.0003
-0.0011	-0.0003	0.0046

Va =

-0.8048	-0.0144	-0.5934
-0.5926	-0.0386	0.8046
-0.0345	0.9992	0.0225

Da =

-0.0266	0	0
0	0.0047	0
0	0	0.0219

South of Los Angeles Block

Strike: Calculated using a plate boundary strike of N42°W

Dip: Vertical

Rake: 180 (right lateral)

Fault Surface Area: 3613.4 km^2

Slip Rate: 47 mm/yr

Depth: 14.0 km

Block volume: 2.7028e+6 km^3

M =

1.0e+26 *

0	-5.6044	0
-5.6044	0	0
0	0	0

SR =

0	-0.0314	0
-0.0314	0	0
0	0	0

V =

-0.7071	0	-0.7071
-0.7071	0	0.7071
0	1.0000	0

D =

-0.0314	0	0
0	0	0
0	0	0.0314

MsumS =

1.0e+26 *

-0.9318	-4.6876	0.2257
-4.6876	0.8885	-0.1002
0.2257	-0.1002	0.0433

SRS =

-0.0052	-0.0263	0.0013
-0.0263	0.0050	-0.0006
0.0013	-0.0006	0.0002

Vs =

0.7717	-0.0121	0.6359
0.6356	0.0506	-0.7704
-0.0228	0.9986	0.0468

Ds =

-0.0269	0	0
0	0.0002	0
0	0	0.0267

MsumA =

1.0e+26 *

-0.9208	-3.7189	0.1985
-3.7189	0.8818	-0.0908
0.1985	-0.0908	0.0390

SRA =

-0.0052	-0.0208	0.0011
-0.0208	0.0049	-0.0005
0.0011	-0.0005	0.0002

Va =

0.7861	-0.0115	0.6180
0.6175	0.0562	-0.7845
-0.0257	0.9984	0.0513

Da =

-0.0216	0	0
0	0.0002	0
0	0	0.0214

Table P5 – Input data for strain tensors and line integrals

Fault sections are assigned the following numbers so that it is easier to account for what faults are in what strain tensors or line integrals.

Section Name	sect #
Green Valley (So)	1
Mount Diablo Thrust	2
Concord	3
Calaveras (No)	4
Calaveras (Central)	5
Greenville (No)	6
Greenville (So)	7
Monte Vista-Shannon	8
Ortigalita	9
Rinconada	10
Monterey Bay-Tularcitos	11
San Gregorio (No)	12
Mendocino	13
Honey Lake	14
Table Bluff	15
Little Salmon (Offshore)	16
Little Salmon (Onshore)	17
Big Lagoon-Bald Mtn	18
Trinidad	19
Fickle Hill	20
McKinleyville	21
Mad River	22
Collayomi	23
Bartlett Springs	24
Rodgers Creek	25
San Andreas (Offshore)	26
San Andreas (North Coast)	27
San Jacinto (Superstition Mtn)	28
San Gregorio (So)	29
Hosgri	30
San Juan	31
San Andreas (Parkfield)	32
Gillem-Big Crack	33
Cedar Mtn-Mahogany Mtn	34
Likely	35
Surprise Valley	36
Hat Creek-McArthur-Mayfield	37
Robinson Creek	38
Mono Lake	39
Hartley Springs	40
Hilton Creek	41
Round Valley	42
Fish Slough	43
White Mountains	44
Death Valley (No of Cucamonga)	45
Death Valley (No)	46
Owl Lake	47
Garlock (East)	48
Garlock (West)	49
Hunter Mountain-Saline Valley	50
Deep Springs	51
Point Reyes	52
Zayante-Vergeles	53
Quien Sabe	54
Calaveras (So)	55
San Andreas (Santa Cruz Mtn)	56
San Andreas (Creeping Segment)	57
Pleito	58
So Sierra Nevada	59
Owens Valley	60
Independence	61
Birch Creek	62
San Andreas (Peninsula)	63
Hayward (No)	64
Hayward (So)	65
West Napa	66
Green Valley (No)	67
Hunting Creek-Berryessa	68
Battle Creek	69
Los Osos	70
San Luis Range (So Margin)	71
Lions Head	72
Santa Ynez (West)	73
Mission Ridge-Arroyo Parida-Santa Ana	74
Santa Ynez (East)	75
San Cayetano	76
Cleghorn	77
North Frontal (West)	78
North Frontal (East)	79
Helendale-So Lockhart	80
Lenwood-Lockhart-Old Woman Springs	81
Gravel Hills-Harper Lk	82
Blackwater	83
Calico-Hidalgo	84
Pisgah-Bullion Mtn-Mesquite Lk	85
So Emerson-Copper Mtn	86
Johnson Valley (No)	87
Landers	88
Pinto Mtn	89
Burnt Mtn	90

Eureka Peak	91
Elmore Ranch	92
Imperial	93
Superstition Hills	94
San Jacinto (Borrego)	95
San Jacinto (Coyote Creek)	96
Elsinore (Julian)	97
Elsinore (Coyote Mountain)	98
Laguna Salada	99
San Jose	100
Hollywood	101
Palos Verdes	102
Santa Rosa Island	103
Santa Cruz Island	104
Verdugo	105
Sierra Madre (San Fernando)	106
Sierra Madre	107
Simi-Santa Rosa	108
Oak Ridge (Onshore)	109
Ventura-Pitas Point	110
Red Mountain	111
San Jacinto (San Bernardino)	112
Coronado Bank	113
Newport-Inglewood (Offshore)	114
Rose Canyon	115
Clamshell-Sawpit	116
Cucamonga	117
Channel Islands Thrust	118
Northridge	119
Great Valley 1	120
Great Valley 3, Mysterious Ridge	121
Great Valley 2	122
Great Valley 4a, Trout Creek	123
Great Valley 5, Pittsburg Kirby Hills	124
Great Valley 7	125
Great Valley 8	126
Great Valley 10	127
Great Valley 11	128
Great Valley 12	129
Great Valley 14 (Kettleman Hills)	130
Great Valley 13 (Coalinga)	131
San Joaquin Hills	132
Little Lake	133
Tank Canyon	134
Elysian Park (Upper)	135
Carson Range (Genoa)	136
Antelope Valley	137
Maacama-Garberville	138
Goose Lake	139
Great Valley 9	140
Raymond	141
Casmalia (Orcutt Frontal)	142
Los Alamos-West Baseline	143
Pitas Point (Lower, West)	144
Pitas Point (Lower)-Montalvo	145
Anacapa-Dume, alt 1	146
Malibu Coast, alt 1	147
Santa Monica, alt 1	148
Santa Susana, alt 1	149
Holser, alt 1	150
Newport-Inglewood, alt 1	151
Whittier, alt 2	152
Chino, alt 1	153
Puente Hills	154
Panamint Valley	155
Death Valley (Black Mtns Frontal)	156
Death Valley (So)	157
San Gabriel	158
Earthquake Valley	159
White Wolf	160
San Andreas (San Bernardino N)	161
San Andreas (San Bernardino S)	162
San Andreas (San Gorgonio Pass-Garnet Hill)	163
San Andreas (Cholame) rev	164
San Andreas (Mojave N)	165
San Andreas (Big Bend)	166
San Jacinto (San Jacinto Valley) rev	167
San Jacinto (San Jacinto Valley, stepover)	168
San Jacinto (Anza, stepover)	169
San Jacinto (Clark) rev	170
San Jacinto (Anza) rev	171
San Andreas (Coachella) rev	172
Elsinore (Glen Ivy) rev	173
Elsinore (Glen Ivy stepover)	174
Elsinore (Temecula stepover)	175
Elsinore (Temecula) rev	176
San Andreas (Carrizo) rev	177
San Andreas (Mojave S)	178
West Tahoe	179
North Tahoe	180
Garlock (Central)	181
Great Valley 4b, Gordon Valley	182
Czone_Foothill_Flt_Sys	183
Czone_Mohawk_Honey_Lake	184
Czone_NE_Cal	185
Czone_Western_Nevada	186
Czone_ECSZ	187
Czone_Imperial_Valley	188
Czone_San_Gorgonio_Knot	189

Columns below are:
1) Section id corresponding to the section name above
2) Average strike
3) Dip
4) Slip rate (mm/yr)
5) Rake
6) Area (km^2)

Entire box fault list

1	-13.90394173	90.0	5.0	180.0	352.2605374
2	-49.1812574	38.0	2.0	90.0	325.1186408
3	-26.30146625	90.0	4.0	180.0	274.9149512
4	156.6543651	90.0	6.0	180.0	587.701315
5	149.2044787	90.0	15.0	180.0	647.8842615
6	146.1013812	90.0	2.0	180.0	397.9174292
7	152.1869967	90.0	2.0	180.0	353.5976168
8	124.616856	45.0	0.4	90.0	223.2353262
9	150.1407721	90.0	1.0	180.0	771.4763872
10	143.3101458	90.0	1.0	180.0	1907.732537
11	-40.71480928	90.0	0.5	150.0	1168.202861
12	158.0271488	90.0	7.0	180.0	1315.361936
14	-49.89690553	90.0	2.5	180.0	631.7722196
23	-33.29049806	90.0	0.6	180.0	284.866272
24	-29.72039639	90.0	6.0	180.0	2610.370283
25	-29.55398905	90.0	9.0	180.0	748.3496166
27	-35.20740864	90.0	24.0	180.0	2082.92384
28	119.5330218	90.0	5.0	180.0	325.8234224
29	-23.69506075	90.0	3.0	180.0	795.1433645
30	-31.45025707	80.0	2.5	180.0	1182.228217
31	152.7601348	90.0	1.0	180.0	880.2721048
32	-40.06046446	90.0	34.0	180.0	371.5908331
33	2.639363974	60.0	1.0	-90.0	412.7778823
35	-39.09484109	90.0	0.3	180.0	703.7458117
36	-8.469508945	50.0	1.3	-90.0	1093.999405
37	166.6909233	60.0	1.5	-90.0	1071.51036
38	27.60097107	50.0	0.5	-90.0	283.0106569
39	-17.32529623	50.0	2.5	-90.0	436.119332
40	-16.40517436	50.0	0.5	-90.0	418.5515684
41	-28.26264248	50.0	2.5	-90.0	497.3720676
42	-19.63609881	50.0	1.0	-90.0	734.7058252
43	-0.763531401	50.0	0.2	-90.0	440.6973324
44	-8.155249112	90.0	1.0	180.0	1438.322766
45	-38.13955154	90.0	5.0	-150.0	998.3320045
46	-39.47764013	90.0	5.0	180.0	1384.998125
47	57.5799599	90.0	2.0	0.0	302.3648728
48	90.97338746	90.0	3.0	0.0	519.2524931
49	58.68246799	90.0	6.0	0.0	1434.369921
50	-42.70915639	90.0	2.5	-150.0	897.186127
51	-155.4450827	50.0	0.8	-90.0	429.8624005
52	-52.95645863	50.0	0.3	90.0	557.1501174
53	-53.83569315	90.0	0.1	150.0	694.410828
54	-35.81342396	90.0	1.0	180.0	228.4533227
55	-19.36050843	90.0	15.0	180.0	212.6143623
56	-48.23350832	90.0	17.0	180.0	931.622146
57	137.0467275	90.0	34.0	180.0	1461.712439

58	90.96516861	46.0	2.0	90.0	823.8165132
59	1.648681567	50.0	0.1	-90.0	1996.236994
60	-18.63193849	90.0	1.5	180.0	1156.944725
61	-29.13491508	50.0	0.2	-90.0	1028.809314
62	-23.72819163	50.0	0.7	-90.0	262.7874641
63	-36.43547045	90.0	17.0	180.0	1098.740252
64	-33.78942937	90.0	9.0	180.0	417.7729511
65	-37.54659649	90.0	9.0	180.0	629.4265908
66	-21.46254698	90.0	1.0	180.0	295.6716887
67	-11.80178756	90.0	5.0	180.0	196.7419607
68	-26.42025354	90.0	6.0	180.0	715.7943749
69	75.2161373	75.0	0.5	-90.0	330.6193806
70	118.1932757	45.0	0.5	90.0	627.9021117
71	-53.45414684	45.0	0.2	90.0	901.6030524
72	-60.94741837	75.0	0.02	90.0	428.2089517
73	91.53917223	70.0	2.0	0.0	660.4970173
74	85.97858425	70.0	0.4	90.0	556.7324572
75	81.79635089	70.0	2.0	0.0	967.4692671
76	-87.46279808	42.0	6.0	90.0	1005.025735
77	97.42274035	90.0	3.0	0.0	391.8568763
78	81.0430746	49.0	1.0	90.0	1043.012394
79	96.56236988	41.0	0.5	90.0	677.9678743
80	-39.12921405	90.0	0.6	180.0	1459.194151
81	-46.7459093	90.0	0.9	180.0	1915.824787
82	-48.64022845	90.0	0.7	180.0	741.9517328
83	-35.10899493	90.0	0.5	180.0	719.9929387
84	-37.5802822	90.0	1.8	180.0	1624.325036
85	-30.08623793	90.0	0.8	180.0	1158.807383
86	-38.60003052	90.0	0.6	180.0	761.8356905
87	-39.10629038	90.0	0.6	180.0	559.7724348
88	-30.01951978	90.0	0.6	180.0	1427.15399
89	85.22576491	90.0	2.5	0.0	1147.810881
90	174.5662819	67.0	0.6	180.0	364.698984
91	-15.03776157	90.0	0.6	180.0	282.7409352
92	-140.3402293	90.0	1.0	0.0	330.5337807
94	130.0261945	90.0	4.0	180.0	455.8638615
95	133.0591279	90.0	4.0	180.0	448.4687641
96	132.7847548	90.0	4.0	180.0	681.5267123
97	-54.21481916	84.0	5.0	180.0	1426.064922
98	-54.72870569	82.0	4.0	180.0	517.2782765
100	-115.5014465	74.0	0.5	30.0	322.7750225
101	-103.5286384	70.0	1.0	30.0	309.8676158
102	-37.487553	90.0	3.0	180.0	1347.941142
103	-88.83687151	90.0	1.0	30.0	500.518891
104	98.20113999	90.0	1.0	30.0	919.0425243
105	-59.4703495	55.0	0.5	90.0	513.4860698
106	-80.72085333	45.0	2.0	90.0	332.5567324
107	-71.36903256	53.0	2.0	90.0	1011.960387
108	-104.490274	60.0	1.0	30.0	501.7696116
109	69.26845481	65.0	4.0	90.0	1001.423579
110	-96.91243096	64.0	1.0	60.0	681.8182794
111	-88.49559245	56.0	2.0	90.0	1709.590867
112	135.4487212	90.0	6.0	180.0	725.7316865
113	146.5658988	90.0	3.0	180.0	1602.234945
114	136.892991	90.0	1.5	180.0	677.5214596
115	-22.34428898	90.0	1.5	180.0	538.0570886
116	-116.2164686	50.0	0.5	90.0	293.2582356
117	-102.9544062	45.0	5.0	90.0	308.8457378

118	-95.53554943	20.0	1.5	90.0	1263.025782
119	111.2067365	35.0	1.5	90.0	546.4077678
120	177.8707637	15.0	0.1	90.0	438.7774436
121	157.2347183	20.0	1.25	90.0	751.4722058
122	-177.4361483	15.0	0.1	90.0	219.814698
123	155.0240167	20.0	1.25	90.0	280.2728708
124	158.9503977	90.0	1.0	180.0	318.9877681
125	134.1495367	15.0	1.5	90.0	447.8304393
126	158.509447	15.0	1.5	90.0	409.7238976
127	152.044083	15.0	1.5	90.0	216.6055935
128	131.4158411	15.0	1.5	90.0	245.7755835
129	152.7743111	15.0	1.5	90.0	175.20183
130	125.243537	22.0	1.5	90.0	922.2551011
131	136.0738421	15.0	1.5	90.0	743.7333501
132	114.3710172	23.0	0.5	90.0	730.0961398
133	-32.32791145	90.0	0.7	180.0	516.1473104
134	-179.1153138	50.0	1.0	-90.0	173.0268
135	-74.77190832	50.0	1.3	90.0	315.7264484
136	-4.787476878	50.0	2.0	-90.0	902.3629356
137	-18.92809284	50.0	0.8	-90.0	697.5579714
138	-30.75838308	90.0	9.0	180.0	2650.92268
139	167.3110345	50.0	0.1	-90.0	742.9481705
140	147.1231386	15.0	1.5	90.0	391.534555
141	-102.0156306	79.0	1.5	60.0	357.2379105
142	115.9631537	75.0	0.25	90.0	300.7047166
143	121.3539072	30.0	0.7	90.0	555.4398079
144	-86.88273588	13.0	2.5	90.0	1127.167395
145	-90.68338948	16.0	2.5	90.0	1349.133993
146	-95.58631598	45.0	3.0	60.0	1115.785685
147	-86.88902897	75.0	0.3	30.0	305.0807665
148	-107.1865129	75.0	1.0	30.0	267.3928918
149	-81.00101994	55.0	5.0	90.0	540.6694611
150	97.14864255	58.0	0.4	90.0	430.0512147
151	-41.18499123	88.0	1.0	180.0	980.5495407
152	-66.26707221	75.0	2.5	150.0	674.8205057
153	145.5857064	50.0	1.0	150.0	285.8834667
154	-69.61224038	25.0	0.7	90.0	835.6808537
155	-26.20413101	90.0	2.5	-150.0	1424.455959
156	166.169094	60.0	4.0	-150.0	1141.450665
157	-39.08392655	90.0	4.0	180.0	544.5739578
158	-50.88756761	61.0	1.0	180.0	1198.650564
159	126.7503977	90.0	2.0	180.0	382.7808363
160	50.72426682	75.0	2.0	60.0	957.6234018
161	121.5025573	90.0	22.0	180.0	451.939471
162	119.6950615	90.0	16.0	180.0	555.4873932
163	-70.15887366	58.0	10.0	180.0	842.9906736
164	-38.77273545	90.0	34.0	180.0	750.1661168
165	109.0983977	90.0	27.0	180.0	556.4521839
166	107.8265824	90.0	34.0	180.0	751.0052959
167	132.5664412	90.0	18.0	180.0	297.2277484
168	133.7954068	90.0	9.0	180.0	389.4844726
169	133.6890589	90.0	9.0	180.0	418.6002533
170	123.9291666	90.0	14.0	180.0	786.1407635
171	126.3629159	90.0	18.0	180.0	775.3124464
172	134.3923341	90.0	20.0	180.0	770.4324219
173	128.4342973	90.0	5.0	180.0	340.8997751
174	125.6662397	90.0	2.5	180.0	147.7212713
175	121.9282013	90.0	2.5	180.0	167.2703989

176	139.8740358	90.0	5.0	180.0	567.6202284
177	134.2110011	90.0	34.0	180.0	891.2256909
178	115.5150341	90.0	29.0	180.0	1278.981072
179	-9.650717124	50.0	0.6	-90.0	870.3468101
180	17.3334952	50.0	0.43	-90.0	332.1269999
181	71.01763089	90.0	7.0	0.0	1276.136888
182	161.8312481	20.0	1.25	90.0	416.0902731
183	-35	75	0.1	-150	4320
184	-45	90	4	180	1320
186	-45	90	8	180	3675
187	-47	90	4	180	3285
188	-35	90	10	180	1134
189	-67	90	4	180	1836

Entire box partial faults

Ratios of how much of fault is in the box in order of list below
[8/9, 3/4, 3/4, 3/10, 1/2]

26	-21.77760019	90.0	24.0	180.0	1497.568185
34	-13.31002153	60.0	1.0	-90.0	852.9483267
93	-34.82908488	82.0	20.0	180.0	674.6529593
99	-49.22951965	90.0	3.5	180.0	1322.89065
185	-25	90	4	180	3450

North box fault list

1	-13.90394173	90.0	5.0	180.0	352.2605374
2	-49.1812574	38.0	2.0	90.0	325.1186408
3	-26.30146625	90.0	4.0	180.0	274.9149512
4	156.6543651	90.0	6.0	180.0	587.701315
5	149.2044787	90.0	15.0	180.0	647.8842615
6	146.1013812	90.0	2.0	180.0	397.9174292
7	152.1869967	90.0	2.0	180.0	353.5976168
8	124.616856	45.0	0.4	90.0	223.2353262
9	150.1407721	90.0	1.0	180.0	771.4763872
11	-40.71480928	90.0	0.5	150.0	1168.202861
12	158.0271488	90.0	7.0	180.0	1315.361936
14	-49.89690553	90.0	2.5	180.0	631.7722196
23	-33.29049806	90.0	0.6	180.0	284.866272
24	-29.72039639	90.0	6.0	180.0	2610.370283
25	-29.55398905	90.0	9.0	180.0	748.3496166
27	-35.20740864	90.0	24.0	180.0	2082.92384
29	-23.69506075	90.0	3.0	180.0	795.1433645
33	2.639363974	60.0	1.0	-90.0	412.7778823
35	-39.09484109	90.0	0.3	180.0	703.7458117
36	-8.469508945	50.0	1.3	-90.0	1093.999405
37	166.6909233	60.0	1.5	-90.0	1071.51036
38	27.60097107	50.0	0.5	-90.0	283.0106569
39	-17.32529623	50.0	2.5	-90.0	436.119332
40	-16.40517436	50.0	0.5	-90.0	418.5515684
52	-52.95645863	50.0	0.3	90.0	557.1501174
53	-53.83569315	90.0	0.1	150.0	694.410828
54	-35.81342396	90.0	1.0	180.0	228.4533227
55	-19.36050843	90.0	15.0	180.0	212.6143623
56	-48.23350832	90.0	17.0	180.0	931.622146
57	137.0467275	90.0	34.0	180.0	1461.712439
63	-36.43547045	90.0	17.0	180.0	1098.740252

64	-33.78942937	90.0	9.0	180.0	417.7729511
65	-37.54659649	90.0	9.0	180.0	629.4265908
66	-21.46254698	90.0	1.0	180.0	295.6716887
67	-11.80178756	90.0	5.0	180.0	196.7419607
68	-26.42025354	90.0	6.0	180.0	715.7943749
69	75.2161373	75.0	0.5	-90.0	330.6193806
120	177.8707637	15.0	0.1	90.0	438.7774436
121	157.2347183	20.0	1.25	90.0	751.4722058
122	-177.4361483	15.0	0.1	90.0	219.814698
123	155.0240167	20.0	1.25	90.0	280.2728708
124	158.9503977	90.0	1.0	180.0	318.9877681
125	134.1495367	15.0	1.5	90.0	447.8304393
126	158.509447	15.0	1.5	90.0	409.7238976
127	152.044083	15.0	1.5	90.0	216.6055935
128	131.4158411	15.0	1.5	90.0	245.7755835
129	152.7743111	15.0	1.5	90.0	175.20183
136	-4.787476878	50.0	2.0	-90.0	902.3629356
137	-18.92809284	50.0	0.8	-90.0	697.5579714
138	-30.75838308	90.0	9.0	180.0	2650.92268
139	167.3110345	50.0	0.1	-90.0	742.9481705
140	147.1231386	15.0	1.5	90.0	391.534555
179	-9.650717124	50.0	0.6	-90.0	870.3468101
180	17.3334952	50.0	0.43	-90.0	332.1269999
182	161.8312481	20.0	1.25	90.0	416.0902731
183	-35	75	0.1	-150	4320
184	-45	90	4	180	1320
186	-45	90	8	180	3675

North box partial faults

Ratios of how much of fault is in the box in order of list below
[2/7, 8/9, 12/25, 1/2, 3/4, 3/5, 1/3, 1/2]

10	143.3101458	90.0	1.0	180.0	1907.732537
26	-21.77760019	90.0	24.0	180.0	1497.568185
30	-31.45025707	80.0	2.5	180.0	1182.228217
32	-40.06046446	90.0	34.0	180.0	371.5908331
34	-13.31002153	60.0	1.0	-90.0	852.9483267
41	-28.26264248	50.0	2.5	-90.0	497.3720676
131	136.0738421	15.0	1.5	90.0	743.7333501
185	-25	90	4	180	3450

South box fault list

28	119.5330218	90.0	5.0	180.0	325.8234224
31	152.7601348	90.0	1.0	180.0	880.2721048
42	-19.63609881	50.0	1.0	-90.0	734.7058252
43	-0.763531401	50.0	0.2	-90.0	440.6973324
44	-8.155249112	90.0	1.0	180.0	1438.322766
45	-38.13955154	90.0	5.0	-150.0	998.3320045
46	-39.47764013	90.0	5.0	180.0	1384.998125
47	57.5799599	90.0	2.0	0.0	302.3648728
48	90.97338746	90.0	3.0	0.0	519.2524931
49	58.68246799	90.0	6.0	0.0	1434.369921
50	-42.70915639	90.0	2.5	-150.0	897.186127
51	-155.4450827	50.0	0.8	-90.0	429.8624005
58	90.96516861	46.0	2.0	90.0	823.8165132
59	1.648681567	50.0	0.1	-90.0	1996.236994

60	-18.63193849	90.0	1.5	180.0	1156.944725
61	-29.13491508	50.0	0.2	-90.0	1028.809314
62	-23.72819163	50.0	0.7	-90.0	262.7874641
70	118.1932757	45.0	0.5	90.0	627.9021117
71	-53.45414684	45.0	0.2	90.0	901.6030524
72	-60.94741837	75.0	0.02	90.0	428.2089517
73	91.53917223	70.0	2.0	0.0	660.4970173
74	85.97858425	70.0	0.4	90.0	556.7324572
75	81.79635089	70.0	2.0	0.0	967.4692671
76	-87.46279808	42.0	6.0	90.0	1005.025735
77	97.42274035	90.0	3.0	0.0	391.8568763
78	81.0430746	49.0	1.0	90.0	1043.012394
79	96.56236988	41.0	0.5	90.0	677.9678743
80	-39.12921405	90.0	0.6	180.0	1459.194151
81	-46.7459093	90.0	0.9	180.0	1915.824787
82	-48.64022845	90.0	0.7	180.0	741.9517328
83	-35.10899493	90.0	0.5	180.0	719.9929387
84	-37.5802822	90.0	1.8	180.0	1624.325036
85	-30.08623793	90.0	0.8	180.0	1158.807383
86	-38.60003052	90.0	0.6	180.0	761.8356905
87	-39.10629038	90.0	0.6	180.0	559.7724348
88	-30.01951978	90.0	0.6	180.0	1427.15399
89	85.22576491	90.0	2.5	0.0	1147.810881
90	174.5662819	67.0	0.6	180.0	364.698984
91	-15.03776157	90.0	0.6	180.0	282.7409352
92	-140.3402293	90.0	1.0	0.0	330.5337807
94	130.0261945	90.0	4.0	180.0	455.8638615
95	133.0591279	90.0	4.0	180.0	448.4687641
96	132.7847548	90.0	4.0	180.0	681.5267123
97	-54.21481916	84.0	5.0	180.0	1426.064922
98	-54.72870569	82.0	4.0	180.0	517.2782765
100	-115.5014465	74.0	0.5	30.0	322.7750225
101	-103.5286384	70.0	1.0	30.0	309.8676158
102	-37.487553	90.0	3.0	180.0	1347.941142
103	-88.83687151	90.0	1.0	30.0	500.518891
104	98.20113999	90.0	1.0	30.0	919.0425243
105	-59.4703495	55.0	0.5	90.0	513.4860698
106	-80.72085333	45.0	2.0	90.0	332.5567324
107	-71.36903256	53.0	2.0	90.0	1011.960387
108	-104.490274	60.0	1.0	30.0	501.7696116
109	69.26845481	65.0	4.0	90.0	1001.423579
110	-96.91243096	64.0	1.0	60.0	681.8182794
111	-88.49559245	56.0	2.0	90.0	1709.590867
112	135.4487212	90.0	6.0	180.0	725.7316865
113	146.5658988	90.0	3.0	180.0	1602.234945
114	136.892991	90.0	1.5	180.0	677.5214596
115	-22.34428898	90.0	1.5	180.0	538.0570886
116	-116.2164686	50.0	0.5	90.0	293.2582356
117	-102.9544062	45.0	5.0	90.0	308.8457378
118	-95.53554943	20.0	1.5	90.0	1263.025782
119	111.2067365	35.0	1.5	90.0	546.4077678
130	125.243537	22.0	1.5	90.0	922.2551011
132	114.3710172	23.0	0.5	90.0	730.0961398
133	-32.32791145	90.0	0.7	180.0	516.1473104
134	-179.1153138	50.0	1.0	-90.0	173.0268
135	-74.77190832	50.0	1.3	90.0	315.7264484
141	-102.0156306	79.0	1.5	60.0	357.2379105
142	115.9631537	75.0	0.25	90.0	300.7047166

143	121.3539072	30.0	0.7	90.0	555.4398079
144	-86.88273588	13.0	2.5	90.0	1127.167395
145	-90.68338948	16.0	2.5	90.0	1349.133993
146	-95.58631598	45.0	3.0	60.0	1115.785685
147	-86.88902897	75.0	0.3	30.0	305.0807665
148	-107.1865129	75.0	1.0	30.0	267.3928918
149	-81.00101994	55.0	5.0	90.0	540.6694611
150	97.14864255	58.0	0.4	90.0	430.0512147
151	-41.18499123	88.0	1.0	180.0	980.5495407
152	-66.26707221	75.0	2.5	150.0	674.8205057
153	145.5857064	50.0	1.0	150.0	285.8834667
154	-69.61224038	25.0	0.7	90.0	835.6808537
155	-26.20413101	90.0	2.5	-150.0	1424.455959
156	166.169094	60.0	4.0	-150.0	1141.450665
157	-39.08392655	90.0	4.0	180.0	544.5739578
158	-50.88756761	61.0	1.0	180.0	1198.650564
159	126.7503977	90.0	2.0	180.0	382.7808363
160	50.72426682	75.0	2.0	60.0	957.6234018
161	121.5025573	90.0	22.0	180.0	451.939471
162	119.6950615	90.0	16.0	180.0	555.4873932
163	-70.15887366	58.0	10.0	180.0	842.9906736
164	-38.77273545	90.0	34.0	180.0	750.1661168
165	109.0983977	90.0	27.0	180.0	556.4521839
166	107.8265824	90.0	34.0	180.0	751.0052959
167	132.5664412	90.0	18.0	180.0	297.2277484
168	133.7954068	90.0	9.0	180.0	389.4844726
169	133.6890589	90.0	9.0	180.0	418.6002533
170	123.9291666	90.0	14.0	180.0	786.1407635
171	126.3629159	90.0	18.0	180.0	775.3124464
172	134.3923341	90.0	20.0	180.0	770.4324219
173	128.4342973	90.0	5.0	180.0	340.8997751
174	125.6662397	90.0	2.5	180.0	147.7212713
175	121.9282013	90.0	2.5	180.0	167.2703989
176	139.8740358	90.0	5.0	180.0	567.6202284
177	134.2110011	90.0	34.0	180.0	891.2256909
178	115.5150341	90.0	29.0	180.0	1278.981072
181	71.01763089	90.0	7.0	0.0	1276.136888
187	-47	90	4	180	3285
188	-35	90	10	180	1134
189	-67	90	4	180	1836

South box partial faults

Ratios of how much of fault is in the box in order of list below
[5/7, 13/25, 1/2, 2/5, 3/4, 3/10, 2/3]

10	143.3101458	90.0	1.0	180.0	1907.732537
30	-31.45025707	80.0	2.5	180.0	1182.228217
32	-40.06046446	90.0	34.0	180.0	371.5908331
41	-28.26264248	50.0	2.5	-90.0	497.3720676
93	-34.82908488	82.0	20.0	180.0	674.6529593
99	-49.22951965	90.0	3.5	180.0	1322.89065
131	136.0738421	15.0	1.5	90.0	743.7333501

San Francisco box fault list

1	-13.90394173	90.0	5.0	180.0	352.2605374
3	-26.30146625	90.0	4.0	180.0	274.9149512

14	-49.89690553	90.0	2.5	180.0	631.7722196
64	-33.78942937	90.0	9.0	180.0	417.7729511
66	-21.46254698	90.0	1.0	180.0	295.6716887
67	-11.80178756	90.0	5.0	180.0	196.7419607
123	155.0240167	20.0	1.25	90.0	280.2728708
124	158.9503977	90.0	1.0	180.0	318.9877681
182	161.8312481	20.0	1.25	90.0	416.0902731

San Francisco box partial faults

Ratios of how much of fault is in the box in order of list below
[1/2, 1/8, 1/4, 1/3, 2/3, 3/7, 2/3, 1/5, 3/4, 1/2, 1/2, 1/5, 1/3]

2	-49.1812574	38.0	2.0	90.0	325.1186408
4	156.6543651	90.0	6.0	180.0	587.701315
6	146.1013812	90.0	2.0	180.0	397.9174292
12	158.0271488	90.0	7.0	180.0	1315.361936
25	-29.55398905	90.0	9.0	180.0	748.3496166
27	-35.20740864	90.0	24.0	180.0	2082.92384
52	-52.95645863	50.0	0.3	90.0	557.1501174
63	-36.43547045	90.0	17.0	180.0	1098.740252
65	-37.54659649	90.0	9.0	180.0	629.4265908
68	-26.42025354	90.0	6.0	180.0	715.7943749
121	157.2347183	20.0	1.25	90.0	751.4722058
183	-35	75	0.1	-150	4320
186	-45	90	8	180	3675

North of San Francisco box fault list

23	-33.29049806	90.0	0.6	180.0	284.866272
24	-29.72039639	90.0	6.0	180.0	2610.370283
33	2.639363974	60.0	1.0	-90.0	412.7778823
35	-39.09484109	90.0	0.3	180.0	703.7458117
36	-8.469508945	50.0	1.3	-90.0	1093.999405
37	166.6909233	60.0	1.5	-90.0	1071.51036
69	75.2161373	75.0	0.5	-90.0	330.6193806
120	177.8707637	15.0	0.1	90.0	438.7774436
122	-177.4361483	15.0	0.1	90.0	219.814698
138	-30.75838308	90.0	9.0	180.0	2650.92268
139	167.3110345	50.0	0.1	-90.0	742.9481705
184	-45	90	4	180	1320

North of San Francisco box partial faults

Ratios of how much of fault is in the box in order of list below
[1/3, 8/9, 4/7, 3/4, 1/2, 1/2, 1/2, 1/3]

25	-29.55398905	90.0	9.0	180.0	748.3496166
26	-21.77760019	90.0	24.0	180.0	1497.568185
27	-35.20740864	90.0	24.0	180.0	2082.92384
34	-13.31002153	60.0	1.0	-90.0	852.9483267
68	-26.42025354	90.0	6.0	180.0	715.7943749
121	157.2347183	20.0	1.25	90.0	751.4722058
185	-25	90	4	180	3450
186	-45	90	8	180	3675

Los Angeles box fault list

47	57.5799599	90.0	2.0	0.0	302.3648728
48	90.97338746	90.0	3.0	0.0	519.2524931
82	-48.64022845	90.0	0.7	180.0	741.9517328
83	-35.10899493	90.0	0.5	180.0	719.9929387
100	-115.5014465	74.0	0.5	30.0	322.7750225
101	-103.5286384	70.0	1.0	30.0	309.8676158
105	-59.4703495	55.0	0.5	90.0	513.4860698
106	-80.72085333	45.0	2.0	90.0	332.5567324
107	-71.36903256	53.0	2.0	90.0	1011.960387
116	-116.2164686	50.0	0.5	90.0	293.2582356
117	-102.9544062	45.0	5.0	90.0	308.8457378
135	-74.77190832	50.0	1.3	90.0	315.7264484
141	-102.0156306	79.0	1.5	60.0	357.2379105
147	-86.88902897	75.0	0.3	30.0	305.0807665
148	-107.1865129	75.0	1.0	30.0	267.3928918
154	-69.61224038	25.0	0.7	90.0	835.6808537
157	-39.08392655	90.0	4.0	180.0	544.5739578
189	-67	90	4	180	1836

Los Angeles box partial faults

Ratios of how much of fault is in the box in order of list below
[2/3, 8/13, 2/3, 4/9, 4/13, 1/4, 9/14, 1/4, 1/2, 6/7, 1/4, 1/2, 5/7, 3/4, 1/5, 18/19, 4/7, 1/2, 3/5, 2/5, 1/2, 3/5, 3/4, 1/2, 1/4]

77	97.42274035	90.0	3.0	0.0	391.8568763
78	81.0430746	49.0	1.0	90.0	1043.012394
80	-39.12921405	90.0	0.6	180.0	1459.194151
81	-46.7459093	90.0	0.9	180.0	1915.824787
84	-37.5802822	90.0	1.8	180.0	1624.325036
88	-30.01951978	90.0	0.6	180.0	1427.15399
102	-37.487553	90.0	3.0	180.0	1347.941142
108	-104.490274	60.0	1.0	30.0	501.7696116
112	135.4487212	90.0	6.0	180.0	725.7316865
119	111.2067365	35.0	1.5	90.0	546.4077678
132	114.3710172	23.0	0.5	90.0	730.0961398
134	-179.1153138	50.0	1.0	-90.0	173.0268
146	-95.58631598	45.0	3.0	60.0	1115.785685
149	-81.00101994	55.0	5.0	90.0	540.6694611
150	97.14864255	58.0	0.4	90.0	430.0512147
151	-41.18499123	88.0	1.0	180.0	980.5495407
152	-66.26707221	75.0	2.5	150.0	674.8205057
153	145.5857064	50.0	1.0	150.0	285.8834667
155	-26.20413101	90.0	2.5	-150.0	1424.455959
156	166.169094	60.0	4.0	-150.0	1141.450665
158	-50.88756761	61.0	1.0	180.0	1198.650564
161	121.5025573	90.0	22.0	180.0	451.939471
178	115.5150341	90.0	29.0	180.0	1278.981072
181	71.01763089	90.0	7.0	0.0	1276.136888
187	-47	90	4	180	3285

South of Los Angeles box fault list

28	119.5330218	90.0	5.0	180.0	325.8234224
79	96.56236988	41.0	0.5	90.0	677.9678743

85	-30.08623793	90.0	0.8	180.0	1158.807383
86	-38.60003052	90.0	0.6	180.0	761.8356905
87	-39.10629038	90.0	0.6	180.0	559.7724348
89	85.22576491	90.0	2.5	0.0	1147.810881
90	174.5662819	67.0	0.6	180.0	364.698984
91	-15.03776157	90.0	0.6	180.0	282.7409352
92	-140.3402293	90.0	1.0	0.0	330.5337807
94	130.0261945	90.0	4.0	180.0	455.8638615
95	133.0591279	90.0	4.0	180.0	448.4687641
96	132.7847548	90.0	4.0	180.0	681.5267123
97	-54.21481916	84.0	5.0	180.0	1426.064922
98	-54.72870569	82.0	4.0	180.0	517.2782765
113	146.5658988	90.0	3.0	180.0	1602.234945
114	136.892991	90.0	1.5	180.0	677.5214596
115	-22.34428898	90.0	1.5	180.0	538.0570886
159	126.7503977	90.0	2.0	180.0	382.7808363
162	119.6950615	90.0	16.0	180.0	555.4873932
163	-70.15887366	58.0	10.0	180.0	842.9906736
167	132.5664412	90.0	18.0	180.0	297.2277484
168	133.7954068	90.0	9.0	180.0	389.4844726
169	133.6890589	90.0	9.0	180.0	418.6002533
170	123.9291666	90.0	14.0	180.0	786.1407635
171	126.3629159	90.0	18.0	180.0	775.3124464
172	134.3923341	90.0	20.0	180.0	770.4324219
173	128.4342973	90.0	5.0	180.0	340.8997751
174	125.6662397	90.0	2.5	180.0	147.7212713
175	121.9282013	90.0	2.5	180.0	167.2703989
176	139.8740358	90.0	5.0	180.0	567.6202284
188	-35	90	10	180	1134

South of Los Angeles box partial faults

Ratios of how much of fault is in the box in order of list below
[1/3, 5/13, 1/3, 4/9, 9/13, 3/4, 3/4, 1/5, 5/14, 1/2, 3/4, 1/19, 3/7, 1/2, 2/5, 1/5]

77	97.42274035	90.0	3.0	0.0	391.8568763
78	81.0430746	49.0	1.0	90.0	1043.012394
80	-39.12921405	90.0	0.6	180.0	1459.194151
81	-46.7459093	90.0	0.9	180.0	1915.824787
84	-37.5802822	90.0	1.8	180.0	1624.325036
88	-30.01951978	90.0	0.6	180.0	1427.15399
93	-34.82908488	82.0	20.0	180.0	674.6529593
99	-49.22951965	90.0	3.5	180.0	1322.89065
102	-37.487553	90.0	3.0	180.0	1347.941142
112	135.4487212	90.0	6.0	180.0	725.7316865
132	114.3710172	23.0	0.5	90.0	730.0961398
151	-41.18499123	88.0	1.0	180.0	980.5495407
152	-66.26707221	75.0	2.5	150.0	674.8205057
153	145.5857064	50.0	1.0	150.0	285.8834667
161	121.5025573	90.0	22.0	180.0	451.939471
187	-47	90	4	180	3285

References

Aki, K., and Richards, P.G. (1980), Quantitative seismology; Theory and Methods, v. 1, Freeman and Co., New York, 557 p.

Bird, P., and Kagan, Y.Y. (2004), Plate-tectonic analysis of shallow seismicity: Apparent boundary width, beta, corner magnitude, coupled lithosphere thickness, and coupling in seven tectonic settings, *Bull. Seis. Soc. Amer., v. 94,* no. 6, 2380-2399, doi:10.1785/0120030107.

Brown, R.D.Jr., and Wallace, R.E. (1968), Current and historic fault movement along the San Andreas fault between Paicines and Camp Dix, California, *Proceeding, Conference on Geologic Problems of the San Andreas Fault System,* W. R. Dickinson and A. Grantz, Editors, *Stanford University Publ. Geol. Sci., v. 11,* 22-39.

Chen, W.-P., and Molnar, P. (1977), Seismic moments of major earthquakes and the average rate of slip in Central Asia, *Jour. Geophys. Res., v. 82,* no. 20, 2945-2969.

DeMets, C., Gordon, R.G., Argus, D.F., and Stein, S. (1994) Effect of recent revisions to the geomagnetic reversal time-scale on estimates of current plate motions: *Geophys. Res. Let., v. 21,* p. 2191–2194, doi:10.1029/94GL02118.

Burford, R.O. (1988), Retardations in fault creep rates before local moderate earthquakes along the San Andreas fault system, central California, *Pageoph., v. 126,* 499-529.

Burford, R.O., and Harsh, P.W. (1980), Slip on the San Andreas fault in central California from alignment array surveys, *Bull. Seis. Soc. Amer., v. 70*, no. 4, 1233-1261.

Freymueller, J.T., Murray, M.H., Segall, P. and Castillo, D. (1999), Kinematics of the Pacific–North America plate boundary zone, northern California, *Jour. Geophys. Res. v. 104*, 7419–7441.

Galehouse, J.S., and Lienkaemper, J.J. (2003), Inferences drawn from two decades of alignment array measurements of creep on faults in the San Francisco Bay Region, *Bull. Seis. Soc. Amer., v. 93*, 2415-2433.

Goulty, N.R., Burford, R.O., Allen, C.R., Gilman, R., Johnson, C.E. and Keller, R.P. (1978), Large creep events on the Imperial fault, California, *Bull. Seis. Soc. Am., v. 68*, 517-521.

Hudnut, K., and Clark, M. (1989), New slip along parts of the 1968 Coyote Creek fault rupture, California, *Bull. Seis. Soc. Am., v. 79*, 451-465.

Humphreys, E. D., and Weldon, R. J. (1994), Deformation across the Western United States: A local determination of Pacific-North America transform deformation, *Jour. Geophys. Res., v. 99*, 19,975-20,010.

King, C., Nason, R.D., and Burford, R.O. (1977), Coseismic steps recorded on creep meters along the San Andreas fault, *Jour. Geophys. Res., v. 82,* 1655-1662.

Kostrov, B. V. (1974) Seismic moment and energy of earthquakes, and seismic flow of rock, *Izv. Acad. Sci. USSR Phys. Solid Earth I.,* 23-44.

Lienkaemper, J.J., Galehouse, J.S., and Simpson, R.W. (2001), Long-term monitoring of creep rate along the Hayward fault and evidence for a lasting creep response to the 1989 Loma Prieta earthquake, *Geophys. Res. Lett., v. 28*, 2265–2268.

Lienkaemper, J.J., Borchardt, G., and Lisowski, M. (1991), Historical creep rate and potential for seismic slip along the Hayward fault, California, *Jour. Geophys. Res., v. 96*, 18,261-18.283.

Lisowski, M., and Prescott, W.H. (1981), Short-range distance measurements along the San Andreas fault system in central California, 1975 to 1979, *Bull. Seis. Soc. Amer, v. 71*, no. 5, 1607-1624.

Louie, J.N., Allen, C.R., Johnson, D.C., Haase, P.C., and Cohn, S.N. (1985), Fault slip in southern California*, Bull. Seis. Soc. Amer., v. 75*, no. 3, 811-833.

Molnar, P. (1983), Average regional strain due to slip on numerous faults of different orientations, *Jour. Geophys. Res., v. 88,* no. B8, 6430-6432.

Molnar, P., Anderson, R. S., and Anderson, S. P. (2007), Tectonics, fracturing of rock, and erosion, *Jour. Geophys. Res., v. 112,* F03014, doi:10.1029/2005JF000433.

Molnar, P. (1979), Earthquake recurrence intervals and plate tectonics, *Bull. Seis. Soc. Amer., v. 69*, no. 1, 115-133.

Oppenheimer, D.H., Bakun, W.H., and Lindh, A.G. (1990), Slip partitioning on the Calaveras fault, California, and prospects for future earthquakes, *Jour. Geophys. Res., v. 95*, 8483-8498.

Petersen, M.D., Bryant, W.A., Cramer, C.H., Cao, T., Reichle, M.S., Frankel, A.D., Lienkaemper, J.J., McCrory, P.A., and Schwartz, D.P., 1996, Probabilistic seismic hazard assessment for the state of California, California Geological Survey Open-file Report 96-08, *USGS Open-file Report 96-706,* 33 pp.

Prescott, W.H., Lisowski, M., and Savage, S.C. (1981), Geodetic measurement of crustal deformation on the San Andreas, Hayward, and Calaveras faults near San Francisco, California, *Jour. Geophys. Res., v. 86*, no. B11, 10,853-10,869.

Prescott, W.H., and R.O. Burford (1976), Slip on the Sargent fault, *Bull. Seis. Soc. Amer.*, v. *66,* no. 3, 1013-1016.

Schulz, S.S., Mavko, G.M., Burford, R.O., and Stuart, W.D. (1982), Long-term fault creep observations in central California, *Jour. Geophy. Res., v. 87*, no. B8, 6977-6982.

Titus, S.J., DeMets, C., and Tikoff, B. (2005), New slip rate estimates for the creeping segment of the San Andreas fault, California, *Geology, v. 33*, 205-208.

Wallace, R. E., and Roth, E. F. (1967), Rates and patterns of progressive deformation, *in* The Parkfield-Cholame California Earthquakes of June-August 1966, *U. S. Geol. Surv. Prof. Paper 579,* 23-40.

Wdowinski, S., Smith-Konter, B., Boch, Y., and Sandwell, D. (2007), Diffuse intersesimic deformation across the Pacific-North America Plate Boundary, 2007 *Geology, v. 35,* no. 4, 311-314.

Wesson, R. L. (1988), Dynamics of fault creep, *Jour. Geophys. Res., 93*, 8929-8951.

Wilmesher, J. F., and Baker F.B. (1987), Catalog of alignment array measurements in central and southern California from 1983 through 1986, *U.S. Geol. Surv. Open-File Rep. 87–280*, 157 pp.